Nanotechnology

DOI: 10.1002/anie.201000235

Oxide Nanomaterials: Synthetic Developments, Mechanistic Studies, and Technological Innovations

Greta R. Patzke, Ying Zhou, Roman Kontic, and Franziska Conrad*

Keywords:
in situ studies · nanomaterials · nanotechnology · oxides · synthetic techniques

Oxide nanomaterials are indispensable for nanotechnological innovations, because they combine an infinite variety of structural motifs and properties with manifold morphological features. Given that new oxide materials are almost reported on a daily basis, considerable synthetic and technological work remains to be done to fully exploit this ever increasing family of compounds for innovative nano-applications. This calls for reliable and scalable preparative approaches to oxide nanomaterials and their development remains a challenge for many complex nanostructured oxides. Oxide nanomaterials with special physicochemical features and unusual morphologies are still difficult to access by classic synthetic pathways. The limitless options for creating nano-oxide building blocks open up new technological perspectives with the potential to revolutionize areas ranging from data processing to biocatalysis. Oxide nanotechnology of the 21st century thus needs a strong interplay of preparative creativity, analytical skills, and new ideas for synergistic implementations.

From the Contents

1. Introduction

Over the past years, the science of nanomaterials has acquired a new perspective—the high expectations of earlier days are now critically reconsidered with respect to the actual methodological progress and the technological benefits realized.[1] The fascinating field of oxide nanomaterials still has many challenges ready and new discoveries are practically reported on a daily basis[2–6] so that we asked ourselves whilst writing this follow-up article to our previous Review on the topic:[7] "Did we witness seven fat or seven meager years?" Where do we stand in the fabrication, understanding, and implementation of oxide nanomaterials? There is no doubt that overwhelming breakthroughs in oxide nanochemistry have been achieved[8] and it is impossible to fully appreciate them all within a single Review. Therefore, we provide a survey of selected exemplary works that outline the progress in research on oxide nanomaterials covering the period since 2002. We start out with new techniques for the preparation of oxide nanomaterials, then the monitoring of reaction processes with in situ methods, and finally we illustrate the occurrence of new materials properties in nanoscale oxides.

This selection can only be far from complete and moreover, it reflects our strong interest in preparative chemistry: we aim to provide a practical guide to how oxide nanomaterials can be prepared and developed for the technological challenges of the future. The following short synopsis of recent Reviews on trends in nanomaterials research puts the development of nanoscale oxides into a general perspective.

"Life sciences" are becoming more and more intertwined with nanotechnology.[9,10] As this complex interdisciplinary research field is beyond this Review, a few suggestions are given for catching up on current topics:

- Nanomedicine has emerged as a particularly powerful interdisciplinary branch[11] and it raises new therapeutic hopes, for example, for the targeting of tumors through magnetic oxide nanoparticles,[12] in artificial tissue engineering,[13] and even for cutting-edge therapeutic strategies based on gene transfer.[14]
- Nanoparticles are also expected to play a major role in the food sector, for example, in the fields of food packaging and polymeric materials, and nanosensors.[15]
- These applications, however, also raise critical issues regarding potential health-hazard factors of nanomaterials. Such fundamental concerns can only be resolved through detailed studies of their metabolic pathways in organisms.[16]

These developments go hand in hand with the physicochemical and technological aspects of nanomaterials fabrication and use:

- The catalytic[17] and sensing[18] functions offered by nanomaterials are expected to play a major role in solving the key problems of modern society, such as the depletion of energy resources[19] and the limited access to clean water.[20] The required technology can also profit from the application of oxide nanomaterials in photocatalysts and advanced energy systems,[19,21] miniaturized sensors,[18,22] solid oxide fuel cells[23] and other environmentally relevant systems.
- All the aforementioned implementations of nanomaterials would not be feasible without a wide arsenal of chemical[24–27] and biologically assisted methods[28–31] to fabricate compounds with the required morphology, phase, and composition. The need for complex oxide materials as building blocks for many areas of nanotechnology has been widely discussed.[32–37]

[*] Prof. Dr. G. R. Patzke, Dr. Y. Zhou, R. Kontic, F. Conrad
Institute of Inorganic Chemistry, University of Zurich
Winterthurerstrasse 190, 8057 Zurich (Switzerland)
Fax: (+41) 44-635-6802
E-mail: greta.patzke@aci.uzh.ch
Homepage: http://www.patzke.ch

- To fully tap the endless pool of oxide structures and properties, a skillful combination of theoretical and experimental approaches is required[38] to keep up with the rapid developments in nanomaterials production.[39] Crystal structure prediction from first principles and atomic-scale modeling techniques are expected to play a fundamental role in future theoretical concepts for nanomaterials preparation.[40]

The present article is focused on the classic oxide types that have traditionally attracted the most intense technological interest. However, modern oxide research is experiencing a rapid diversification and this introduction would be incomplete without a brief glimpse on what lies ahead (but is beyond the scope of this Review): oxide materials exhibit an ever growing range of structural motifs[41] and they cover a continuum from 3D-solids to large molecules, including the important family of polyoxometalates.[42,43] Oxides are the key components of many hybrids and composites[44,45] and oxide building blocks open up new research horizons in the wide area of framework materials[46] that encompasses an enormous range of representatives, such as metal–organic frameworks (MOFs)[47] or denser hybrid framework structures.[48] Given that even amorphous mixed oxides exhibit useful properties,[49] the future application options for oxide-based materials appear to be endless.

Coming back to the "genuine" oxides that are at the heart of this Review, the crucial questions that keep triggering many studies in the field are how far can we go in the targeted preparation of oxide nanomaterials? and how far can we go in utilizing them in innovative technologies? It seems like preparative nanochemistry has reached a "turning point", because many crucial issues remain unsolved despite years of intense research. For example, we still do not fully understand nucleation and growth processes of nanomaterials in general and this renders their predictive phase and morphology control a demanding task. A huge gap is opening up between the continuous development of macroscopic functional oxide materials and their transfer to nanoscale dimensions. As a result, commercially successful nanotechnologies are lagging behind their counterparts in the macro-world.

Herein, we do our best to tackle the huge task of surveying the nano-oxide field, starting with the state-of-the art in nanoscale oxide synthesis. We focus on solution-based techniques, beginning with inspirational variations of the traditional approaches then covering innovative modifications of them and finally pioneering combined methods.

The choice of examples allows us to compare binary oxides with oxide systems of higher complexity to illustrate the "synthetic bottleneck" that they still have to pass on the way to nanomaterials. Next, we discuss how the boundaries of in situ methods have been pushed to understand the mechanisms behind the formation of oxide nanomaterials. Again, we focus on the challenging topic of monitoring the organization processes of several cations into a well-defined nanoscale oxide with a desired morphology. Finally, we round the discussion off with selected spotlights on cutting-edge and truly "synergistic" technological developments—in which we demonstrate how tailoring oxide nanomaterials paves new ways to the most diverse application fields.

Greta R. Patzke was born in 1974 in Bremen, Germany, and studied chemistry at the University of Hannover. In 1999, she received her PhD under the supervision of Prof. Dr. M. Binnewies before moving to the ETH Zurich (2006) for her Habilitation with Prof. Dr. R. Nesper. Since 2007, she has been Assistant Professor (SNSF, Tenure Track) at the Institute of Inorganic Chemistry, University of Zurich. Her research interests are on the development of new oxide-based materials, ranging from nanomaterials to polyoxometalates to hybrid compounds, with special emphasis on targeted synthesis and current applications.

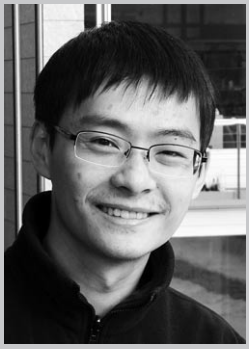

Ying Zhou received his BSc and MSc in materials science from Central South University, China, in 2004 and Shanghai Institute of Optics and Fine Mechanics, Chinese Academy of Sciences, in 2007, respectively. In 2010, he received his PhD under the supervision of Prof. G. R. Patzke. He is currently a postdoctoral researcher (UZH Research Grant) in the same group. His research interests are in the areas of hydrothermal synthesis, in situ studies, and environmental applications of oxide nanomaterials (see section on novel in situ monitoring techniques).

Roman Kontic was born in 1985 in Basel, Switzerland, and studied materials science at the ETH Zurich where he completed a MSc (with Prof. Dr. M. Textor) in 2008. He is currently studying for a PhD at the University of Zurich with Prof. G. R. Patzke. His research interests are the hydrothermal synthesis of nanostructured transition-metal oxides, their morphological and structural investigation, and their photocatalytic properties (see Sections on synthesis and new properties of nano-oxides).

Franziska Conrad was born in 1981 in Potsdam, Germany, and studied chemistry at the University of Potsdam, where she received a diploma (with Prof. Dr. P. Strauch) in 2008. During her studies, she did an internship at CSIRO Australia, Clayton/Melbourne. She is currently a PhD student at the University of Zurich, with Prof. G. R. Patzke. Her research interests are the investigation of nanostructured oxides, especially spinels, and the development of microwave and sonochemistry techniques (see section on synthetic techniques).

2. Synthetic Methods for Oxide Nanomaterials

Over the past centuries, the solid-state synthesis of oxides and nanomaterials thereof has been developed to the highest theoretical and technological levels.[50,51] Although solid-state synthesis is still the method of choice for many preparations of ceramics and other large-scale industrial productions, the targeted preparation of nanomaterials often requires more specialized approaches. New solution-based methods have been developed for this purpose over the past decades and their innovative potential for accessing a wide spectrum of nanoscale oxides is outlined below. In the following, we explicitly focus on low-temperature methods in solution with special emphasis on their most recent developments that have a high potential for time- and energy-saving technical processes. For other interesting approaches to nanomaterials synthesis in high-boiling, coordinating solvents or through aerosol flame synthesis, we would like to refer to other Reviews.[52] The efficiency of high-temperature and gas-phase pathways to complex oxide nanoparticles has also been reviewed elsewhere[53] and pulsed laser deposition techniques furthermore play an important role in the fine-tuning of complex oxide thin films.[54]

2.1. Hydro- and Solvothermal Methods

Hydrothermal and solvothermal techniques are the most prominent and well-established methods for the laboratory and industrial synthesis of nanomaterials.[24,55–58] The production of nanomaterials with facile autoclave syntheses offers many advantages, such as operational temperatures well below the melting point of the reactants, a multitude of autoclave types, and tunable reaction parameters. They provide access to metastable phases and to nanoscale morphologies that are otherwise difficult to obtain. However, this experimental versatility also renders the planning and understanding of hydrothermal processes a considerable challenge, because their mechanistic principles still remain to be fully understood and to be embedded into a general theoretical concept. Although hydrothermal methods are extremely useful, especially for the synthesis of oxides and related materials, they may be difficult to control with respect to tailored phases and nanoscale morphologies. Nevertheless, remarkable progress has been achieved in the engineering of autoclave types over the past years so that sophisticated inlet and sensing techniques as well as continuous flow reactors are now available.[24,27,59] In addition to the ongoing development of classic sol–gel processes that are frequently coupled with hydrothermal approaches, non-aqueous routes to oxide nanomaterials attract increasing interest.[60]

Over the past years, a multitude of hydrothermal studies has been focused on the synthesis of oxide-related nanomaterials, starting from the commercially most relevant binary oxides (e.g. SnO_2, ZnO, or TiO_2) over ternary and higher compounds to the new field of metal–organic framework (MOF) materials.[48,61] Herein, we firstly focus on the recent progress in hydrothermal morphology control of oxide nanomaterials, followed by the demanding hydrothermal preparation of nanostructured complex oxides containing two or more metal cations. Table 1 contains a recent literature survey on the topic.

Controlling the shape of the nanoscale particles emerging from a hydrothermal process is a difficult task, given that the problem of singling out the desired phase among many other potential products has to be solved in the first place. Whereas growth processes based on anisotropic structural features are very elegant techniques to create anisotropic morphologies, their applicability is inherently limited to specific structure types. Therefore, hydrothermal reactions are often directed with additives towards a specific morphology of the products. Among the vast multitude of organic templates that have been applied in hydrothermal synthesis, natural products and polymers have emerged as abundant, versatile, and generally applicable tools for shaping nanostructured oxides. The hydrothermal preparation of hollow microspheres of binary oxides in the presence of polysaccharides is an instructive example (Figure 1).[62] The carbohydrate additives form microspheres with abundant hydrophilic surface groups in the course of the hydrothermal treatment. The metal ions are subsequently complexed on the surface of the spherical template. Pyrolitic removal of the organic template yields a variety of hollow oxide spheres (Fe_2O_3, NiO, Co_3O_4, CeO_2, MgO, and CuO) and this efficient strategy is likely to be extended to other oxide systems.[62]

Inorganic templates are another convenient option to shape oxides during a hydrothermal reaction, for example, through the interaction of ions with certain facets of the growing nanocrystal or by the selective incorporation of additive ions. This approach is demonstrated in a study from our group on the hydrothermal preparation of hexagonal alkali tungstates in the presence of alkali chlorides:[63] Whereas the smaller alkali cations (Li, Na, K) favor the formation of nanorods or nanofibers, the larger cations (Rb, Cs) support hierarchical arrangements of nanorods into cylindrical and spherical architectures. In this case, a single hydrothermal method generates different morphologies of a technologically interesting oxide type by simply varying the alkali cation (for mechanistic studies on the topic see Section 3).

An impressive example for the synergistic interaction of two different inorganic additives is the hydrothermal synthesis of single crystalline α-Fe_2O_3 nanotubes in the presence of sodium sulfate and sodium phosphate. The phosphate ions induce anisotropic growth along the *c* direction through preferential adsorption on the corresponding crystal planes. Furthermore, a high content of complexing ions in the solution, such as phosphate and sulfate, can lead to the dissolution of the unprotected tips of the growing spindle-like structures. This interplay between dissolution and selective adsorption finally results in the formation of tubular α-Fe_2O_3 nanostructures (Figure 2).[64] These are morphologically rather robust and can thus be transformed into nanotubular Fe_3O_4 and γ-Fe_2O_3 through follow-up thermal redox reactions in a H_2/Ar atmosphere and air, respectively.

Whereas the hydrothermal synthesis of the industrially most relevant binary oxide materials is now well established, it is still far more difficult to direct several oxide precursors

Table 1: Survey of recent hydro- and solvothermal approaches to oxide nanomaterials (target oxides are listed in alphabetical order from binary to higher systems).

Oxide	Solvent/additives	Morphology	Ref.
Morphology control of binary and ternary oxides			
CeO_2, CuO, Co_3O_4, Fe_2O_3, MgO, NiO	water, glucose	nanoparticles, arranged in hollow microspheres	[62]
CuO	water, sodium citrate	nanosheets, -rods, -stars	[69]
Fe_2O_3, Fe_3O_4	water, Na_2SO_4/Na_2HPO_4	short nanotubes	[64]
Fe_3O_4	water/ethanol, oleic acid	nanocubes	[70]
MoO_3	water, acidic and ionic additives	nanorods	[71]
MoO_x	ethanol/water, hexadecylamine	nanoribbons	[72]
SnO, SnO_2	water (HCl/NaOH)	nanoparticles, nanoplatelets (influence of pH)	[73]
SnO_2	water/ethanol	nanorods	[74]
TiO_2	water (NaOH)	nanorods, nanotubes (influence of precursor size/structure)	[75]
TiO_2	water, HCl or acetic acid	nanoparticles (phase selective)	[76]
VO_x	acetone, hexadecylamine	nanotubes	[77]
ZnO:Co/Mn	benzyl alcohol/anisole	nanoparticles, -rods, -fibers (depending on solvent mixture)	[78]
Bi_2WO_6	water, PEO-PPO-PEO (P123)	annular arrangement of nanoparticles	[79]
Bi_2WO_6	water	nanoplatelets in flower like arrangement	[80]
$SrWO_4$	microemulsion: water/cyclohexane/n-pentanol/CTAB	nanoparticles, nanorods	[81]
W/Mo oxides	water, inorganic additives (alkali chlorides)	spherical arrangements	[84]
(earth) alkali vanadates	water, inorganic additives	microrods, fibers	[85]
$K_xMn_{1-y}Co_yO_2$	Water	nanorods, nanoplatelets in flower-like arrangements	[82]
$KTa_{1-x}Nb_xO_3$	water (KOH), PEG	nanocrystals	[83]
Multimetal oxides			
$Ba_{1-x}Sr_xTiO_3$	ethylenediamine/ethanolamine, KOH	nanocrystals (20–40 nm, depending on Sr content)	[95]
$Ba_2MTi_2Nb_3O_{15}$ (M=Nd, Sm)	water, acetic acid	particles with irregular shape (>200 nm)	[93]
$Ca_{1-2x}(Eu,Na)_{2x}WO_4$	water, HNO_3, citric acid, NaOH	nanoparticles with irregular shape (ca. 20–50 nm)	[94]
$Ca_{0.8}Sr_{0.2}Ti_{1-x}Fe_xO_3$	water (KOH); flow reactor	cuboidal nanocrystals (20–30 nm)	[66]
$Ca_2Nb_{2-x}Ta_xO_7$	water	nanoparticles (5–15 nm)	[96]
$Ce_{0.6}Zr_{0.3}Y_{0.1}O_2$	water, urea	nanoparticles (<100 nm)	[86]
$Co_xZn_{1-x}Fe_2O_4$	water (NaOH), PEG	nanoparticles (10–15 nm)	[89]
$La_{0.5}Ca_{0.5}MnO_3$	water (KOH)	single-crystalline nanowires (ca. 80 nm diameter)	[65]
$La_{1-x}Sr_xMO_3$ (M=Co/Mn)	water (NH_3), citric acid	particles with irregular shape (ca. 100 nm)	[88]
$La_{0.8}Sr_{0.2}Ga_{0.8}Mg_{0.2}O_{2.8}$	water, urea	agglomerates of nanoparticles (45 nm, XRD amorphous)	[91]
$LiVMoO_6$	ethanol, N_2H_4	Nanoparticles (50–100 nm)	[90]
$Mn_{1-x}Zn_xFeO_4$	ethylene glycol, sodium acetate, PEG, PVP, CNTs	agglomerates of Nanoparticles (ca. 50 nm)	[97]
MoVTeNb (M1 mixed oxide)	water	wires (100–200 nm diameter)	[68]
Y_2O_3-TiO_2-ZrO_2 solid solution	water	nanoparticles (ca. 50 nm)	[92]
$Y_3Al_5O_{12}$:Eu/Ce	water (NaOH); flow reactor	nanoparticles (60–200 nm, depending on Eu content)	[67, 87]

into a specific complex oxide material and control the morphology. A selected example from the intensely researched area of perovskite materials outlines the successful organization of different cations into a target nanostructure, namely orthorhombic $La_{0.5}Ca_{0.5}MnO_3$ nanowires.[65] Two different manganese-containing precursors ($KMnO_4$ and $MnCl_2$) were combined with lanthanum and calcium nitrate at elevated reaction temperatures (275 °C in a stainless steel autoclave) to afford single-crystalline nanowires with diameters around 80 nm and lengths of several microns. A similar precursor combination (metal nitrates and TiO_2) was used for the continuous-flow synthesis of $Ca_{0.8}Sr_{0.2}Ti_{1-x}Fe_xO_{3-\delta}$ ($x = 0.1$–0.3) in aqueous solution under supercritical conditions.[66] The perovskite-type nanoparticles (ca. 25 nm in diameter) were obtained from basic solutions after a thorough parameter optimization of pH value, iron content, and temperature. Among the multitude of ternary oxides, garnets are another technologically important mixed-oxide type, and recently, a

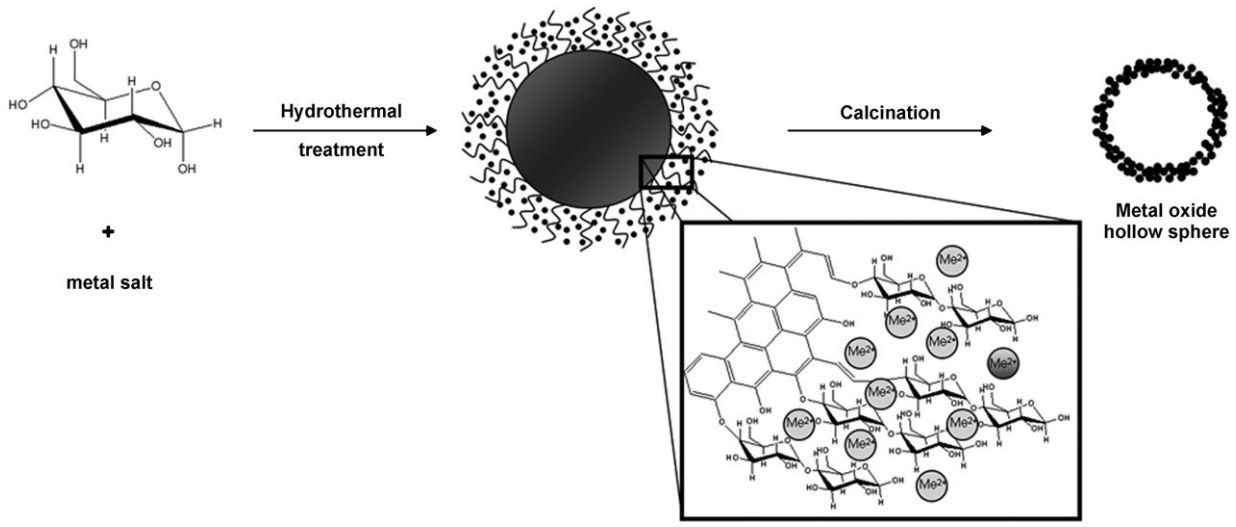

Figure 1. Hydrothermal formation of metal oxide hollow spheres from a polysaccharide-assisted approach. The hydrophilic anchor groups of the polymeric template organize the precursor metal ions into spherical architectures. Reprinted from Ref. [62], with permission. Copyright 2010 American Chemical Society.

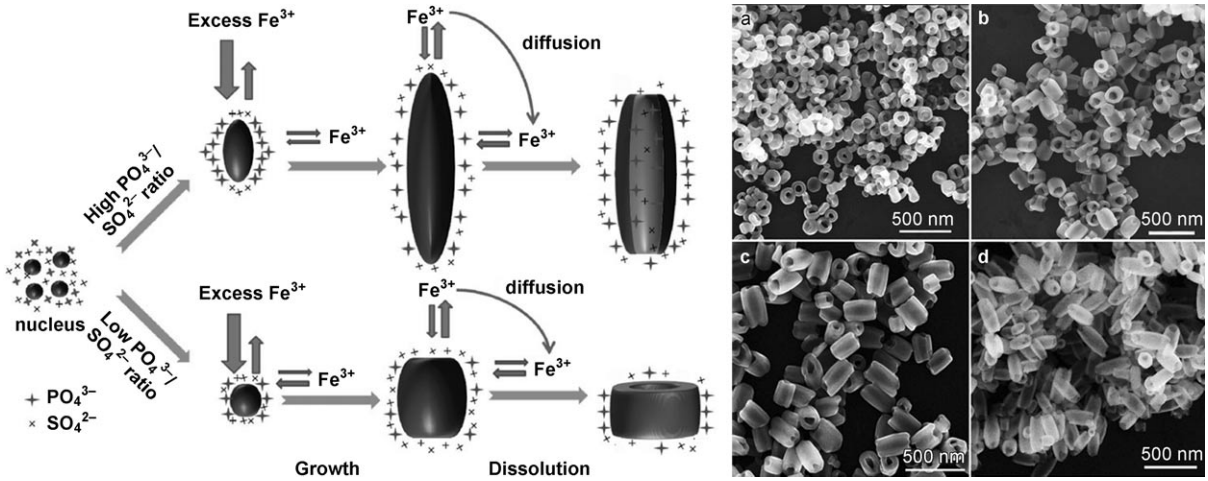

Figure 2. Left: Reaction scheme illustrating the influence of the phosphate and sulfate concentration on the formation of hematite nanotubes. Right: SEM images of α-Fe_2O_3 nanotubes synthesized with different phosphate concentrations: a) 0.1 mM, b) 0.36 mM, c) 0.5 mM, and d) 0.6 mM (the concentrations of Fe^{III} and sulfate ions were kept constant at 20 mM and 0.55 mM, respectively). Reprinted from Ref. [64], with permission. Copyright 2010 American Chemical Society.

continuous-flow synthesis under supercritical conditions of $Y_3Al_5O_{12}$ (yttrium aluminum garnet, YAG) nanoparticles (ca. 80 nm) doped with 10 atom% Eu^{3+} was reported.[67] Again, a basic precursor solution of metal nitrates was used and the nanoparticles were formed after injection into the reactor at 280 bar and 400 °C.

Generally, controlling the synthesis of multicomponent oxides is an important prerequisite for the development of new catalysts. The hydrothermal synthesis of MoVTeNb oxide nanoparticles (M1 phase) illustrates the high degree of selectivity that can be achieved through a carefully tuned hydrothermal process.[68] After a multitude of parameter optimizations, for example, of the reaction time, the temperature, the reactor inlay, and the stirring mode, XANES/EXAFS studies demonstrated that the hydrothermal reaction is the crucial step leading to a homogeneous mixed-oxide phase with all five cations incorporated. Post-treatment at 550 °C then affords a crystalline product for catalytic applications.

In summary, hydrothermal processes have become increasingly attractive over the past years for the synthesis of oxide nanomaterials as a result of their simple and variable setup, their low-cost and "green chemistry" features. Although many questions about their theoretical background still remain open, the limits of hydrothermal synthesis are being pushed towards more and more complex products, because their uncomplicated technical handling permits extensive screening processes allowing the hydrothermal

parameters to be quickly optimized on an empirical basis. However, the "black box" character of this technique remains a fundamental problem that is further discussed in Section 3.

2.2. Microwave-Assisted Strategies

As outlined in the previous Section, the convenient operation of hydrothermal reactions comes at the cost of several disadvantages: one of them is the long initial heating period that may result in inhomogeneous temperature profiles within the autoclave. Microwave-solvothermal processes (MW-ST) overcome these problems by heating the reaction mixture rapidly and homogenously to the desired temperature (Figure 3). Therefore, they open up new options for energy- and cost-saving approaches towards nanoparticles production.[98,99] In addition, this state-of-the-art technique is also time-saving through dramatically increased crystallization kinetics and it provides access to novel or otherwise metastable phases.[100]

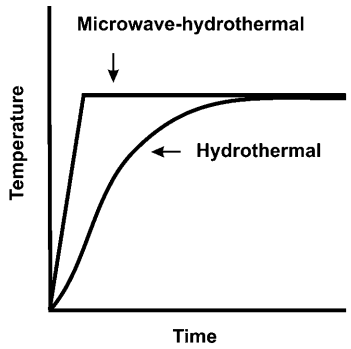

Figure 3. Different heating rates of conventional and microwave-hydrothermal techniques (adapted from Ref. [100]).

The efficiency of microwaves to enhance organic reactions as well as the synthesis of solid materials has been widely demonstrated.[101,102] This effect has been explained on the basis of several hypotheses: in addition to the increase of the net rate through rapid and more uniform heating, microwaves also change the association between reactive species and give rise to superheating phenomena. The creation of "hot spots" and the enhanced dissolution of reactants can furthermore promote the reactivity of microwave-assisted processes.[101]

In the following, we firstly illustrate the rapid development of MW-ST techniques for the synthesis of ZnO, SnO_2, and TiO_2 as key building blocks for nanotechnology, followed by an outlook on new synthetic avenues to other interesting oxide-based materials. A survey of recent literature for further reading can be found in Table 2.

ZnO is one of the most widely investigated oxides in nanomaterials chemistry, because of its unique optical and electronic properties, so that it has been frequently accessed with microwave-assisted methods.[103–106] Among the multitude of publications on the topic, a recent study on the nonaqueous microwave synthesis of ZnO nanoparticles clearly demonstrates the advantages of the microwave-mediated route over conventional synthetic approaches on the basis of kinetic investigations.[103] The direct correlation between the kinetics of the organic side reactions with the growth rate of the nanoscale ZnO products permits the convenient monitoring of the reaction so that the microwave-based process can be quantitatively compared to the slower conventional route (Figure 4).

Given that MW-ST processes offer even more reaction parameters than conventional approaches, methodological investigations are indispensable to explore the full potential of this new synthetic method. The applied microwave power, for example, exerts a tremendous effect on the morphology of the hierarchical ZnO nanostructures emerging from the water/ethylene glycol (EG) system.[105] Another powerful strategy for MW-ST morphology control is variation of the solvent composition, as has been illustrated recently for the formation of ZnO particles in water/EG mixtures:[107] a higher volume ratio of EG restricts the longitudinal growth of the ZnO particles so that their shape can be varied between hexagonal prisms and, for example, peanut-like arrangements. As an additional benefit, the materials obtained display enhanced photocatalytic activity.

Furthermore, an impressive variety of nanoscale ZnO architectures was generated from a low-power/low-temperature MW-ST approach (50 W, 90 °C), followed by an aging procedure (Figure 5).[108] In this case, the morphology-directing parameters were identified as being the precursor, capping agent, and aging time. The wide parameter window for controlling microwave-assisted processes is also evident from a recently reported self-assembly route towards ZnO nanostructures using triethanolamine (TEA) which has a dual function—namely as a capping agent and for adjusting the pH value. The pH value is the key parameter to vary the morphology from raspberry-like arrangements to hollow spheres and both product types were formed within a remarkably short reaction time of 90 seconds.[109]

The wide application spectrum of TiO_2 in daily life (e.g. in paints and cosmetics) and in advanced technologies (such as in gas sensors, self-cleaning surfaces, or photocatalysts) arises from its unique combination of nontoxicity, low chemical reactivity, and outstanding optical properties. Consequently, numerous microwave-based studies on the synthesis of TiO_2 nanoparticles have been published over the past years.[110–119] The interplay between anatase and rutile formation has been investigated in great detail, especially with respect to the influence of reaction temperature, microwave irradiation, and organic solvents.[113] In principle, both polymorphs can be formed simultaneously or selectively within a few minutes of microwave irradiation.

Although the use of organic media amplifies the product spectrum of microwave techniques,[113] their water-based microwave-hydrothermal (MW-HT) operation is certainly the preferable option for industrial processing from the ecological and economic point of view.[120] Nevertheless, a comparison of various microwave-mediated routes to TiO_2 nanoparticles,[113,121] clearly demonstrates the strong dependence of the resulting polymorph and its morphology on slight variations of the solvent mixture. As there is no general MW-

Table 2: Synthesis of oxide nanomaterials with microwave-assisted techniques (MW = microwave, ST = solvothermal, HT = hydrothermal; see discussion in Section 2.2.).

Oxide	Technique	Morphology/special features	Ref.
ZnO	non-aqueous sol-gel MW approach	kinetic correlation between organic reaction process and ZnO particle growth	[103]
	MW-ST with ethylene glycol	bundles, flower-like morphologies and microspheres depending on heating parameters	[105]
	Co-doped ZnO MW-ST with ethylene glycol	nanopowders (particle size <50 nm)	[106]
	MW-ST with ethylene glycol	variety of ZnO nanoparticles (rods, spheres, peanut-shaped...) depending on ethylene glycol content	[107]
	MW-HT and MW-ST, different precursors and various solvents/capping agents	wide nanoparticle spectrum (rods, needles, disks, star-shapes, spheres etc.)	[108]
	MW synthesis using triethanolamine as capping agent	spherical, raspberry-like and hollow spherical nanostructures by self-assembly of Zn^{2+} ionic complexes	[109]
	MW-ST using hexamethylenetetramine (HMT)	ZnO rods with various morphologies like bi-, tri- and tetrapods, oriented growth	[145]
	MW-HT	zincite structure	[146]
	MW synthesis using hydrazine and ammonia	flower shapes with hydrazine and spherical particles with ammonia (wurtzite structure)	[147]
	MW-HT	nanoneedles on a flexible substrate (Teflon) upon addition of $AlCl_3$	[148]
TiO_2	MW-HT in diluted HCl	rutile, shuttle-like morphology	[110]
	MW-HT starting from colloidal titania suspensions	spherical particles (10 nm) and acicular grains (100 nm × 10 nm)	[111]
	MW using EtOH and acetic acid	selective or simultaneous formation of anatase and rutile	[113]
	MW-HT with urea and $TiOCl_2$	anatase phase, agglomerated spherical particles (10 nm)	[114]
	MW-HT	nanotubes, inner pore diameters around 4 nm and BET up to 360 $m^2 g^{-1}$	[116]
	MW-HT, before aging	nanotubes, anatase or rutile or mixed phases, diameters of 8–12 nm and lengths up to 200–1000 nm	[117]
	MW-HT	anatase, crystallites 5 nm, high BET	[118]
	sol-gel MW non-aqueous	anatase, platelet-like shape, 15 nm	[119]
	MW-HT	mixed phases and rutile through longer reaction times, spherical and needle-shaped rutile particles	[121]
SnO_2	microwave flash synthesis	nanoparticles (ca. 5 nm), high BET	[124]
	aqueous MW synthesis	spherical particles, size ≈10 nm, platelet-like particles or pseudo-spherical morphology (diam. 26–34 nm)	[125]
	dip-coating from MW synthesized colloidal suspensions	SnO_2 thin films	[126]
	MW-HT	cassiterite structure, ≈25 nm, faceted grains (almost square shaped)	[127]
	sol-gel MW	in situ formation of amorphous carbon from decomposition of citrate precursor (particle size 15–18 nm)	[128]
	MW-ST	microporous spheres (diameter ≈4 nm)	[129]
	MW with reflux (water and urea)	nanoparticles (size ca. 3 nm)	[130]
$BaTiO_3$	MW-HT	spherical particles with diameters between 30 and 100 nm	[115]
Bi_2WO_6	MW-HT	nanoplates, photocatalytic activity for degradation of methylene blue ($\lambda > 400$ nm)	[135]
CoO, ZnO, Fe_3O_4, MnO, Mn_3O_4 and $BaTiO_3$	MW-ST in benzyl alcohol	different particle morphologies and varying degree of uniformity	[133]
α-Fe_2O_3	MW-HT	nanorings with outer diameter of 100 and inner diameters from 20 to 60 nm	[132]
In_2O_3:Sn	MW with polyols	nanoparticles (average size ca. 17 nm)	[123]
$La_2W_{2-x}Mo_xO_9$	MW synthesis using ultrapure graphitic carbon	detailed structural investigations for solid state, MW synthesis explorations	[136]
Mo-V-Te-Nb-O system	MW-HT	small cylinder-shaped crystallites, catalytic investigations	[144]
TiO_2-SiO_2	microwave-induced combustion process	nanoparticles 10–20 nm in size, anatase phase	[134]

ST "recipe" for either anatase or rutile formation in sight, further mechanistic and parameter studies are required (see Section 3).

The specific surface area of a given TiO_2 material is another crucial parameter that needs to be optimized in solvothermal methods, and the complex interplay between the various synthetic options in MW-ST and the resulting materials parameters is illustrated in a study on the formation of Ti-based nanotubes and nanoribbons:[116] conventional hydrothermal routes afford nanotubular trititanate with an

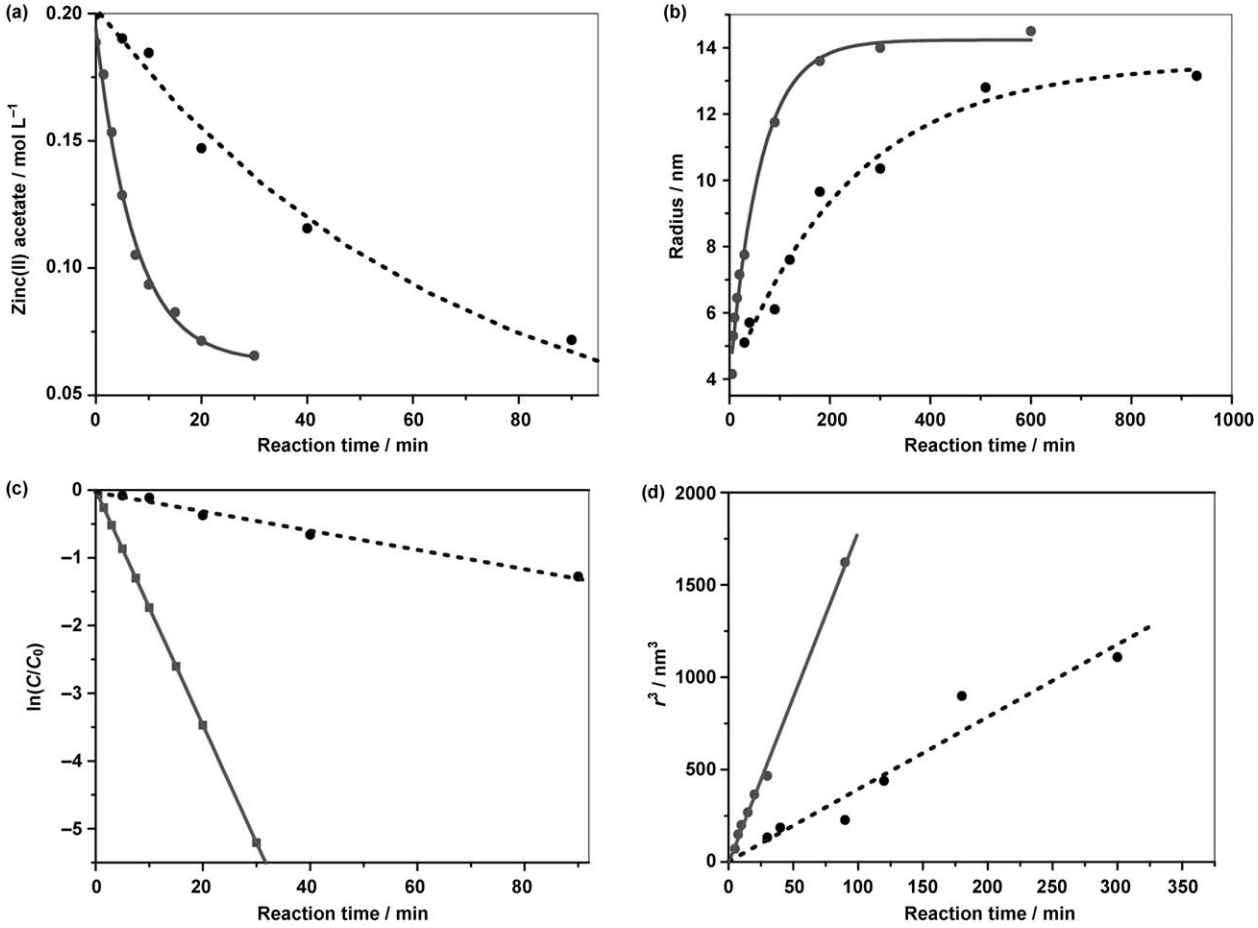

Figure 4. Comparison of benzyl acetate (a, c) and ZnO formation (b, d) using microwave (solid line) and conventional heating (dotted line) at 120 °C. a) Zinc acetate concentration versus reaction time, c) corresponding first-order kinetic plot. b) Radius of the ZnO nanocrystals versus reaction time, d) r^3 versus time according to the LSW (Lifshitz–Slyozov–Wagner) model. Reprinted from Ref. [103], with permission. Copyright 2010 American Chemical Society.

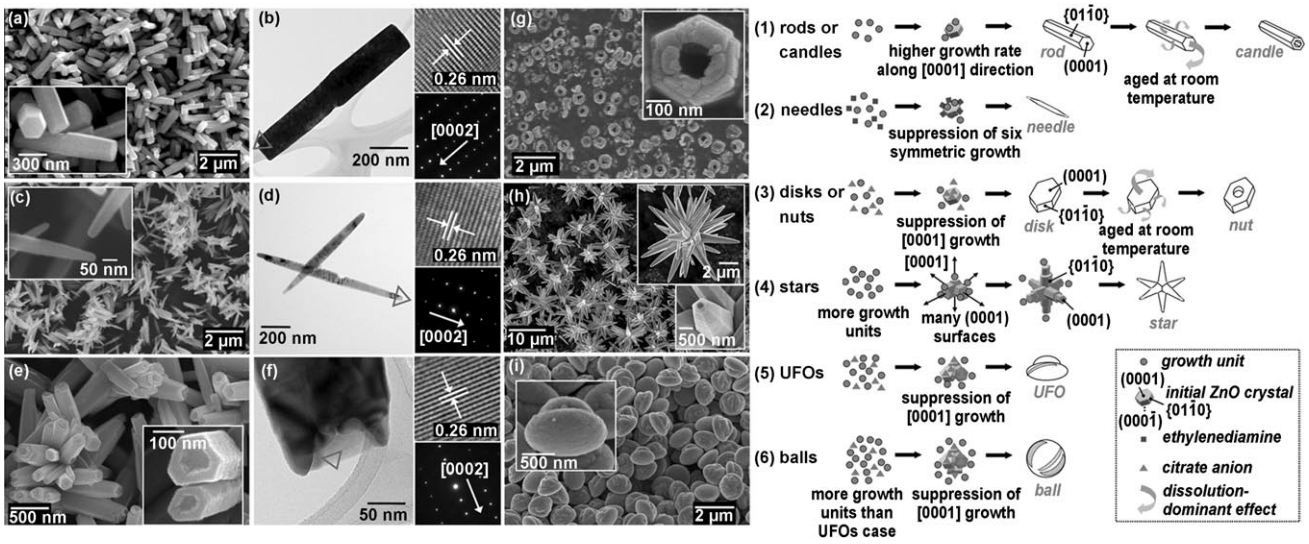

Figure 5. Left: Representative SEM (a, c, e, g–i), TEM (b, d, f), and SAED (insets in b, d, f) images illustrating the morphology tuning of ZnO with MW-ST processes. Right: Proposed growth schemes for the different morphologies. Reprinted from Ref. [108], with permission. Copyright 2010 American Chemical Society.

impressive surface area of $360\,m^2g^{-1}$ and inner pore size diameters around 4 nm. Although the application of MW-HT synthesis lowers the surface area due to the formation of anatase nanoribbons with closed ends, the phase change from trititanate to anatase increases the photocatalytic activity of the products considerably.

SnO_2 is a well-investigated n-type semiconductor with a wide band gap that offers a balanced combination of chemical, optical, and electronic properties resulting in an impressive range of applications, for example, in catalysts, heat mirrors, transparent electrodes for solar cells, optoelectronic devices, liquid-crystal displays, and especially in gas sensors with a high sensitivity towards flammable or toxic gases. Therefore, various groups have reported microwave-assisted routes to SnO_2.[122–130] One of them demonstrates how the technical potential of MW-ST approaches can be explored through the construction of special microwave ovens that induce higher field strengths within the samples than the commercially available models.[124] As a result, the reaction temperatures are reached very quickly, thereby reducing the reaction times to only 60 seconds. The resulting SnO_2 nanoparticles are around 5 nm in diameter and their high BET surfaces (up to $191\,m^2g^{-1}$) makes them promising for gas-sensor applications.[124] Pre-treatments of the precursors can further enhance the efficiency of MW-ST syntheses as has been shown in a combined sol–gel/MW-ST approach to SnO_2 nanoparticles.[128] The decomposition of a $SnCl_2{\cdot}H_2O$/citric acid complex into carbon-containing species may shorten the reaction time and prevent particle agglomeration (Figure 6).

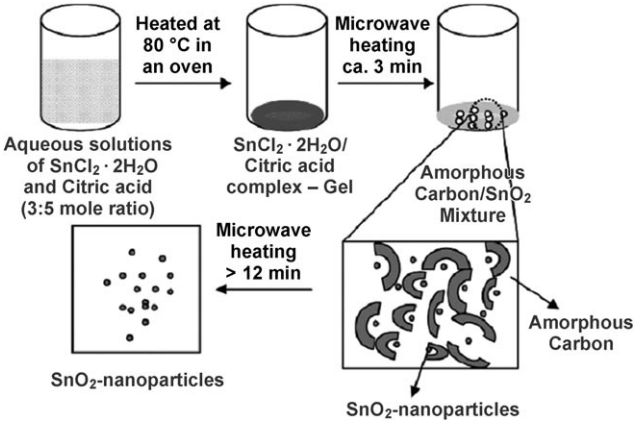

Figure 6. Combination of sol–gel with MW-ST techniques for the formation of SnO_2 nanoparticles. Reprinted from Ref. [128], with permission. Copyright 2010 American Chemical Society.

The corresponding reference experiment using conventional heating procedures failed to produce SnO_2 particles of comparable quality. As outlined below in more detail, the most efficient routes to oxide nanoparticles are often based on combinations of two different synthetic strategies to generate a "synergistic" effect.

The synthesis of nanoscale crystalline materials with micropores[131] is a particularly challenging task in contemporary nanomaterials chemistry. It has been mastered for microporous SnO_2 nanoparticles using a novel surfactant-assisted microwave synthesis with cetyltrimethylammonium bromide (CTAB).[129] The resulting particle morphology depends on the CTAB concentration and the morphology-determining reaction step is the arrangement of Sn^{4+} ions around 3D micelles of the surfactant. As zinc and iron oxides could be obtained by the same route, it has the potential to become a general microwave-based approach to microporous materials.

Microwave-assisted syntheses are currently being explored for the synthesis of numerous other oxides and the following examples illustrate the wide spectrum of target materials ranging from binary functional oxides to the more complex ternary ones. The formation of α-Fe_2O_3 nanorings sheds light on the superheating and nonthermal effects during microwave-assisted processes.[132] In this context, the occurrence of "hot spots" is widely discussed as a reason for microwave-induced nucleation, crystal growth, and the formation of seeds. As for the hematite nanorings, a nucleation–aggregation–dissolution sequence is proposed with the assembly of nanodisks into nanorings in the final step (Figure 7).

Figure 7. Proposed formation model for α-Fe_2O_3 nanorings (top) and the corresponding SEM and TEM images (bottom).[132]

Microwave-assisted techniques in non-aqueous reaction media are exceptionally versatile, as illustrated by the one-minute synthesis of binary and ternary metal oxide nanoparticles, such as CoO, ZnO, Fe_3O_4, MnO, Mn_3O_4, and $BaTiO_3$.[133] TiO_2/SiO_2 oxide mixtures have also been accessed with microwave methods, as these are particularly interesting targets because they combine the excellent semiconductor and catalyst features of TiO_2 with the chemical and mechanical resistance of SiO_2. The resulting composites find application as photocatalysts for hydrogen production by water splitting as well as in antireflection and protective coatings. Recent studies showed that MW-ST strategies are superior to other synthetic methods for preparing TiO_2/SiO_2 materials containing phase-pure anatase nanoparticles.[134]

Bi_2WO_6 is another material with highly promising photocatalytic properties that were further enhanced through the

synthesis of nanostructured particles by MW-ST methods.[135] For this purpose, the reaction parameters (especially pH value, concentration, and temperature) had to be carefully optimized and the holding time, as well as the temperature, turned out to exert the most significant influence on the course of the reaction (for more detailed discussions on Bi_2WO_6 nanoparticle formation see Section 3).

Generally, substitution reactions between tungsten and molybdenum are an elegant way of optimizing oxide materials containing these elements, and the structural implications of such processes were investigated in great detail for compounds of the $La_2W_{2-x}Mo_xO_9$ type.[136] In the course of this study, a microwave-assisted solid-state approach to these mixed oxides was developed, starting from La_2O_3, MoO_3, and WO_3 embedded into ultrapure graphitic carbon that was removed through thermal post-treatment after the reaction (1 h at 1000 °C).[136]

A case study from our laboratory illustrates how microwave hydrothermal methods can give oxide phases that are difficult to access with conventional methods—even as bulk materials. In the present case, copper gallium spinels were obtained with a straightforward MW-HT approach, but, in addition, this strategy also produced nanostructured materials which was recently demonstrated by some of us for copper-substituted $ZnGa_2O_4$ spinels.[137] Copper gallium spinels are interesting materials from the theoretical and technical point of view: the Cu^{2+} ions which display the Jahn–Teller effect, are distributed within the "inert" gallium sublattice and they can be reductively transformed into nanoscale copper-catalysts that are embedded in the gallium matrix. Nevertheless, only few syntheses of copper gallium spinel phases have been reported to date, namely solid-state,[138] sol–gel,[139a] and a route to a spin-glass state.[139b] The other important phase in the Cu/Ga-oxide system, delafossite $CuGaO_2$, is more readily available, it can be prepared by pulsed laser deposition as thin films[140] and by a solvothermal route.[141] As our first attempts to isolate the spinel phase through the solvothermal reaction of copper and gallium salts in ethylene glycol failed, we modified the synthetic strategy into a MW-HT approach by applying copper and gallium salts, water, and ammonia (25 %) to adjust the pH value between 10.5 and 10.7. Through this fine-tuning of the reaction conditions, we finally obtained nanostructured spinel-type copper gallium oxides (Figure 8) within a few minutes at comparatively mild temperatures. The pH window of the reaction is extremely narrow and pH values below 10 led to the formation of impurities. Concerning the reaction temperature, the MW-HT synthesis of the copper gallium oxide nanospinels can be performed between 150 and 180 °C, because the tolerance towards temperature changes is higher compared to the restrictive pH limits. Finally, the role of the precursor is less decisive, because mixtures of sulfates and nitrates both lead to phase-pure copper gallate products with identical morphologies. Interestingly, the nanostructured copper gallium oxide spinel-type particles display a high stability towards thermal post-treatment: both phase and morphology are maintained up to 700 °C.

Europium-doped yttrium aluminum garnet (YAG:Eu^{3+}) as another key oxide material can not only be accessed through conventional hydrothermal synthesis (see above),

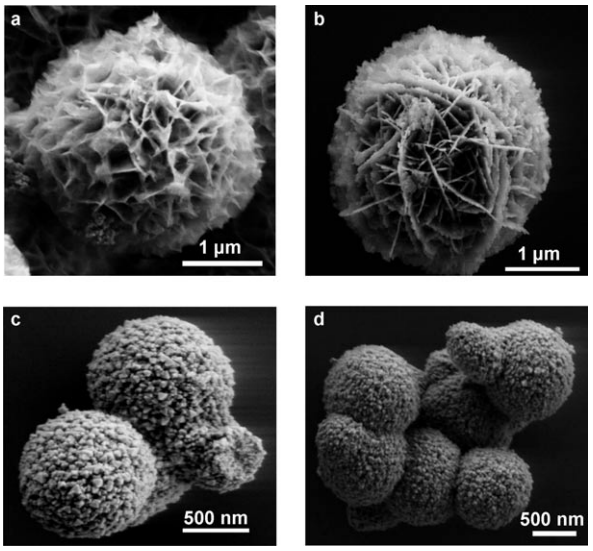

Figure 8. Representative SEM images of copper gallium spinels: a) MW-HT at 130 °C, b) HT at 180 °C for 48 h, c) MW-HT at 180 °C, and d) sample (c) calcinated at 600 °C for 2 h.

but also by a polyol-assisted microwave route.[142] 1,4-Butanediol turned out to be the optimal surface stabilizer during the reaction, because it limits the particle growth and prohibits agglomeration. Finally, the Mo-V-Te-Nb-O system[68] has not only been accessed with hydrothermal and spray-drying methods,[143] but also with microwave irradiation as a heat source.[144] In this case, the MW-approach led to the formation of the M1 phase with an interesting open structure and high catalytic activity. This remarkable phase selectivity within a complex oxide system illustrates the high potential of microwave-assisted routes in the convenient and reliable synthesis of mixed nanostructured oxides.

Generally, microwave syntheses offer many advantages in materials synthesis: they are time- and energy-saving and they provide a straightforward access to phases and morphologies that are difficult to obtain with conventional techniques. These features makes them an attractive option for future large-scale production processes. However, the theoretical background of microwave procedures is even less well understood than the principles behind conventional hydrothermal syntheses. The in situ monitoring of microwave techniques and the elucidation of their special features (such as "hot spots") opens up a challenging new research field for scientists worldwide with plenty of room for creative experimental designs.

2.3. Sonochemical Methods

Sonochemical methods employ ultrasound irradiation—typically in the range from 20 kHz to 500 MHz—to initiate or to alter chemical processes. Although ultrasonic effects (in the following: US) were first described in the beginning of the 20th century and have been widely used in cleaning facilities ever since, a general interest in their preparative use was only developed in the 1980s.[149] The chemical effects of ultrasound

irradiation arise from cavitation phenomena: sound waves travel as alternating compression and rarefaction fronts through the liquid. When the ultrasound power is sufficiently high, the decompression during the rarefaction overcomes the intermolecular forces within the medium so that tiny bubbles are formed, which almost instantaneously collapse again. At least three different regions or reaction zones occur during this collapse phase in the bulk solution: firstly, the centers of the bubbles are characterized by extremely high energy densities leading to local effective temperatures as high as 5000 °C and pressures of 1000 bar and more in the moment of collapse. Secondly, the temperatures and pressures at the bubble–liquid interfaces are still elevated, albeit not as high as in the center. Thirdly, intensive shear forces act on large molecules or complexes located in the vicinity of the collapsing bubble.[149–153]

The collapse of a bubble close to an extended surface, however, is an anisotropic process resulting in a high-speed jet of liquid towards of the surface, that can, in principle, induce erosion or fracture, depending on the local materials properties. This effect is frequently utilized, for example, in cleaning processes or heterogeneous catalysis.[151–153] Sonochemical reaction rates depend on the irradiation frequency and geometry, on the acoustic power and also on the volatility of the solvent which influences the cavitation strength. Solvents with a higher volatility generally lead to more frequent yet weaker cavitations because of a cushioning effect of the gas phase inside the collapsing bubble, whereas the cavitation strength is reinforced by higher external pressure and lower temperatures. As dissolved molecules are potential nucleation sites for cavitation, the reaction mixture should be degassed prior to the experiment. Alternatively, a steady gas flow through the reaction mixture can keep the influence of the dissolved gas constant.[149,152,153] From the preparative point of view, sonochemical approaches are advantageous, because they speed up reaction rates and they favor the formation of porous products and high BET surfaces and have the additional economic benefit of relatively low reaction temperatures. Special attention, however, must be paid to their strong dependency on the ultrasound power and to the fact that the synthesis of highly anisotropic particles may sometimes be difficult. Similarly, the quantitative conversion of the starting materials into crystalline products is another issue that may require further optimization.[154] In the following, we illustrate the versatility of sonochemical methods for selected syntheses of binary and ternary oxide materials and a more detailed summary can be found in Table 3.

The sonochemical deposition of ZnO and CuO nanoparticles on textiles has recently been launched on an industrial scale for the biocidal coating of various fabrics. Starting from acetate precursors, small particles (10–20 nm in size) adhere firmly to the textile surfaces and retain their antibacterial activity even after repeated washing cycles.[155]

From the synthetic point of view, the cavitation processes in ultrasound-assisted reactions can be turned into a tool for morphology control through the use of water-soluble nanoparticles with an optimized degree of hydrophobicity. The air/water interface of the emerging bubbles can thus be stabilized through a higher persistence in comparison with surfactants.[156,157] Such pronounced stabilization effects were employed for the ultrasound-driven formation of hollow silica spheres.[158] CTAB was used to render the nanoparticles slightly more hydrophobic and the diameter of the cavitation bubbles was increased with $NaHCO_3$ as an additive. This strategy led to the formation of rather stable hollow spheres, probably through the crystallization and fusion of nanoparticles on the contact sites (Figure 9). Consequently, US irradiation can be used to direct small nanoparticles into well-defined microarchitectures with a narrow size distribution.

Well dispersed $Fe_3O_4@SiO_2$ core–shell nanoparticles (<20 nm) are available from a two-step sonochemical approach through the injection of different precursor materials directly into the active zone below the ultrasonic horn.[159] A black precipitate was formed immediately after the injection of Fe^{II} and Fe^{III} chloride. This intermediate product was magnetically separated, washed, and redispersed with ethanol, followed by the corresponding injection of ethanol/TEOS into the active zone of the sonoreactor to yield the homogeneous $Fe_3O_4@SiO_2$ nanocomposite.

Porous and hollow hematite nanospheres were recently synthesized through the sonication of $[Fe(CO)_5]$ in the presence of carbon nanoparticles as auxiliaries.[160] The carbon nanoparticles are covered with an amorphous layer of iron oxide and the composites self-ignite upon drying in air so that the carbon template burns off to yield α-Fe_2O_3 nanospheres.

An interesting example for the US-based synthesis of ternary oxides is the formation of porous $CeVO_4$ nanoparticles from cerium(III) nitrate and either NH_4VO_3 or V_2O_5.[161] Both precursors afford different morphologies under otherwise identical reaction conditions: ammonium vanadate favors the formation of nanorods (ca. 100 nm in length, 15 nm in diameter, BET surface area 100 $m^2 g^{-1}$) whilst vanadium pentoxide affords spherical nanoparticles (ca. 20 nm, BET surface area 120 $m^2 g^{-1}$). Interestingly, the crucial influence of the vanadium oxide-based precursor in the synthesis of nanostructured vanadates that has been described elsewhere[162,163] still prevails even under the drastic effect of ultrasonication. Another representative US-assisted route to a ternary oxide, namely the spinel phase $ZnFe_2O_4$, demonstrates the efficient use of biphasic solvent systems:[164] the precursor solution of zinc(II) acetate and iron(II) acetate was subjected to ultrasound treatment in a large excess of rapeseed oil (1:25). In the first place, the aqueous precursor solution was finely distributed among the oil droplets and upon prolonged sonication times, increasing reaction temperatures led to the evaporation of the aqueous phase. The emerging zinc ferrite nanoparticles were distributed in rapeseed oil and displayed a homogeneous size distribution around 4 nm.

2.4. Synthesis of oxide nanomaterials with ionic liquids

Whereas all salt melts are ionic liquids in the strict sense of the word, this term has nowadays been reserved for their representatives with a melting point below 100 °C and

Table 3: Sonochemical approaches to oxide nanomaterials (oxides are listed in alphabetical order from binary to higher systems).

Oxide	Solvent, additives	Morphology	Ref.
Bi_2O_3	water (HNO_3/NaOH), PVP	nanoparticles (100–200 nm)	[165]
CeO_2	NaOH(aq), PEG	nanorods (<10 nm diameter)	[166]
Co_3O_4, NiO	water/ethanol (NH_3), CTAB	agglomerates of nanoparticles (100–150 nm)	[167]
Fe_2O_3 (hematite)	hexadecanol	hollow nanospheres (ca. 10 nm)	[160]
Fe_2O_3	tetraethyleneglycole	nanoparticles (ca. 50 nm)	[168]
Fe_3O_4	water, SDS	nanoparticles (ca. 10 nm)	[169]
Fe_3O_4	water/ethanol (NaOH)	nanoparticles (ca. 15–50 nm, depending on solvent)	[170]
Fe_3O_4/SiO_2	water (HCl/NH_3), ethanol	core-shell nanoparticles (15–20 nm)	[159]
MnO_2	LiOH (aq)	nanofibers (5–10 nm diameter)	[171]
Mn_3O_4	LiOH(aq)	nanoparticles (50-150 nm, depending on Mn precursor)	[172]
MoO_3	water, H_2O_2, PEG	nanofibers (<100 nm diameter)	[173]
SnO	water (HCl/NH_3)	nanoparticles with irregular size (ca. 50 nm)	[174]
SiO_2	water, $NaHCO_3$, CTAB	hollow shells of fused nanoparticles (10–40 μm)	[158]
TiO_2 (anatase)	water/ethanol	nanoparticles (<10 nm)	[175]
TiO_2 (rutile)	water (HCl)	short nanorods (ca. 50 nm diameter)	[176]
TiO_2 (rutile)	NaOH(aq)	agglomerates of nanoparticles (50–100 nm)	[177]
ZnO	ethanol (LiOH)	nanoparticles (5–10 nm)	[178]
ZnO	water, hexamethylene triamine	nanorods (ca. 50 nm diameter)	[179]
ZnO	water/DMF	nanodiscs (ca. 300 nm diam., 50–100 nm thick)	[154]
ZnO:Mg	tetraethylene glycol (LiOH)	nanoparticles (<5 nm)	[180]
Bi_2MO_6 (M = Mo, W)	water	nanoparticles (100–200 nm)	[181]
$BiVO_4$	water, PEG	nanoparticles (50–70 nm)	[182]
$CeVO_4$	water (NH_3)	nanoparticles and nanorods, depending on conditions	[161]
$CoCr_2O_4$	water (NH_3)	nanoparticles (30–40 nm)	[183]
$CuAl_2O_4$	water, urea	nanoparticles (10–20 nm)	[184]
$Cu_{1-x}Ni_xWO_4$	Water, CTAB	nanorods or nanoparticles, depending on Ni content	[194]
$LiCoO_2$	LiOH(aq)	flake-like nanoparticle agglomerates (100–200 nm)	[185]
$MgAl_2O_4$	water/propanol (NH_3), CTAB	Irregular nanoparticles (ca. 100 nm)	[187]
$MMeO_4$ (M = Ca, Sr, Ba; Me = Mo, W)	ethylene glycol	nanoparticles (15–20 nm)	[188, 189]
MVO_4 (M = La, Ce, Nd, Sm, Eu, Gd)	water (NaOH), PEG	nanoparticles, nanorods (depending on M)	[190]
$PbWO_4$	water, PEO-PPO-PEO (P123)	hollow spindles (200–300 nm diameter)	[186]
$ZnAl_2O_4$, $ZnGa_2O_4$	water (NH_3)	nanoparticles (ca. 30 nm and ca. 5 nm, respectively)	[191]
$ZnFe_2O_4$	water/rapeseed oil	nanoparticles (ca. 4 nm)	[164, 192]
$ZnWO_4$	water/ethanol, PEO-PPO-PEO (P123)	short nanorods (ca. 20 nm diameter)	[193]

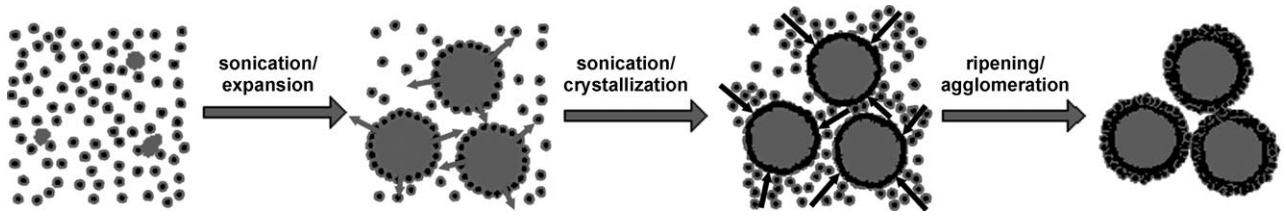

Figure 9. Formation scheme for the ultrasound-assisted growth of hollow silica spheres by nanoparticle fusion around cavitation bubbles.[158]

complex organic or inorganic ions as key ingredients which disfavor crystallization processes. Ionic liquids (ILs; a short glossary of the ILs referred to in this Section is provided in Table 4) display quite interesting properties, such as low viscosity or high thermal and electrochemical stability.[195–198] Their vapor pressures are extremely low, that is, they are nonvolatile and nonflammable under ambient conditions. As the arsenal of constituents for designing ionic liquids keeps growing, especially through the use of functionalized organic ligands, the large family of ionic liquids covers a wide range of physical and chemical properties.[120] Although ionic liquids have been produced for the past fifty years, primarily for electrolyte applications, their tremendous synthetic potential has only been explored for about a decade—this rather slow development bears analogy to the late launch of preparative ultrasonication techniques discussed in the previous Section. These days, ionic liquids find widespread application in organic chemistry and organometallic catalysis,[196–198] whilst

Table 4: Common abbreviations and full chemical names of ionic liquids (ILs) used for the synthesis of oxide nanomaterials.

IL abbreviation	Chemical name
TBAH	tetrabutylammonium hydroxide
[Emim][Br]	1-ethyl-3-methylimidazolium bromide
$[C_2mim][BF_4]$	1-ethyl-3-methylimidazolium tetrafluoroborate
$[C_4mim][SO_3CF_3]$	1-butyl-3-methylimidazolium trifluoromethanesulfonate
$[C_4mim][BF_4]$/[Bmim][BF_4]	1-butyl-3-methylimidazolium tetrafluoroborate
[Bmim][PF_6]	1-butyl-3-methylimidazolium hexafluorophosphate
[Bmim][Cl]	1-butyl-3-methylimidazolium chloride
$[C_4mim][Tf_2N]$	1-butyl-3-methyl-bis(trifluoromethylsulfonyl) imide
$[C_8mim][BF_4]$/[Omim][BF_4]	1-methyl-3-octylimidazolium tetrafluoroborate
$[C_{16}mim][Br]$	1-hexadecyl-3-methylimidazolium bromide
$[MeBu_3N][N(SO_2CF_3)_2]$	methyl tributyl ammonium bis(trifluoromethylsulfonyl) imide
[Bpy][BF_4]	*N*-butylpyridinium tetrafluoroborate

their use in inorganic synthesis is just about to start.[199] This situation is all the more astonishing, given that ionic liquids offer unique possibilities, for example, to work at elevated temperatures without the need for pressure-resistant reaction vessels or to conduct reactions in highly polar solvents under arid conditions. In the following, we present some representative examples for the IL-based synthesis of binary oxides with special emphasis on ZnO, TiO_2, and SnO_2 along the lines of Section 2.2., followed by a glimpse of the full methodological potential of ILs for the synthesis of oxide nanomaterials (see Table 5).

The structure-directing properties of ILs are evident from the facile synthesis of hexagonal ZnO nanopyramids from zinc acetate in a mixture of oleic acid and ethylenediamine.[200] The ionic liquid lowers the surface energy of the polar planes of the zinc precursor so that the hexagonal pyramids are formed as a consequence (Figure 10).

The reaction temperature was used as an efficient morphology-directing factor in the synthesis of various ZnO particles with the assistance of a hydrated ionic liquid precursor, namely TBAH.[201a] At room temperature, ZnO mesocrystals were formed from nanoscale rod-like particles, whereas the morphology changed to hollow mesocrystals at elevated temperatures (100 °C). Contrary to the general observations for nucleation processes in aqueous media, the number of particles in the TBAH/water mixtures decreased within the initial 30 h of the reaction by four orders of magnitude. A slight variation of this method demonstrates the influence of the reaction-vessel material on IL processes, because ZnO mesocrystals with complex morphologies were detected on the glass walls of the reactor.[201b] The direct incorporation of the metal-ion precursor within the ionic liquid is a quite elegant "two in one" option for the straightforward synthesis of oxide nanomaterials.[202,203] In a recent study on the formation of ZnO nanoparticles, the zinc cation was complexed with neutral amine ligands and combined with an established organic counteranion (Scheme 1 a).[203] The combination of ILs with hydrothermal methods is another flexible approach to generate several types of ZnO particles.[204] The choice of the ionic liquid (Scheme 1 b: IL **1**–**4**) exerts a crucial influence on the emerging morphology, as illustrated in Figure 11 for the different products formed in the presence of IL **1** and IL **2**: whereas IL **1** promotes the growth of flower-like ZnO structures consisting of hexagonal prisms with pyramidal tips, the ZnO particles formed in the presence of IL **2** are rod-shaped. It was proposed that the ILs play a multiple role by controlling the particle growth process and inhibiting further agglomeration through the formation of a covering film on the ZnO crystals.[204]

As discussed in previous Sections, the differentiation between the rutile and the anatase (and also the brookite) modification is a crucial task in the synthesis of TiO_2 nanomaterials. As anatase is formed primarily during most solution-based syntheses, a result of its higher thermodynamic stability for particle sizes below 20 nm, the high-temperature modification rutile is usually obtained from the thermal transformation of anatase or brookite. Recently, however, the phase-directing properties of ILs were utilized for the direct synthesis of rutile nanorods under ambient conditions.[205] The formation of rutile is enabled during the non-aqueous sol–gel process through an interaction between the TiO_2 surface and the electron lone pairs on the imide group of the ionic liquid. This interaction is significantly stronger for the (110) crystal plane of rutile than for the anatase form so that rutile formation occurs already at room temperature. The critical step that induces the transformation of the amorphous intermediate into a crystalline phase is the removal of the IL—and the detection of IL residues in the rutile product indicates that the structure-directing interactions are remarkably persistent.[205]

The correlation between the type of ionic liquid and the resulting TiO_2 modification was investigated in detail for the hydrolysis of $TiCl_4$ in a HCl/IL system.[206] The rutile/anatase ratio is strongly influenced by the amount of the IL [Emim][Br], and both modifications differ considerably with respect to their morphologies (anatase nanoparticles of 4–6 nm in size vs. rutile nanorods up to 60 nm in length and 3–6 nm in diameter). The formation of rutile nanorods can again be explained with a specific surface interaction on the (110) facet of rutile and a stacking of imidazole rings (Figure 12) which cannot take place with the anatase structure. To finally obtain phase-pure rutile particles, a minimum HCl concentration of 6 mol/L is required.[206]

Nanoparticles of the gas-sensing oxide SnO_2 cannot only be accessed conveniently through MW-HT methods,[122–130] but also by the incorporation of a room-temperature ionic liquid, such as $[C_{16}mim][Br]$, into a sol–gel process and subsequent heat treatment.[207] Similar to the IL-assisted formation of rutile nanoparticles,[206] this "green chemistry" approach is based on a strong interaction between the IL and tin oxide that is reinforced through hydrogen bonding and the π–π stacking of the imidazolium rings. After calcination of the as-synthesized SnO_2 nanoparticles, they display wormhole-like pores that provide an easy access for sensing gases.

Table 5: Synthetic routes to TiO_2, ZnO, SnO_2 (see Section 2.4.) and other oxides using ionic liquids.

Oxide	Technique	Morphology/feature	Ref.
TiO_2	sol-gel synthesis with [Bmim][PF_6]	anatase, high BET, controlled porosity, high thermal resistance, no anatase-to-rutile transformation	[212]
	sol-gel synthesis with [Bmim][PF_6]	highly porous anatase form with good photocatalytic properties, IL as structure-directing solvent	[213]
	hydrolysis of $TiCl_4$ in HCl using [Emim][Br]	[Emim]Br supports formation of rod-like rutile caused by stacking of IL and growing particles, influence of IL and HCl content important	[206]
	non-aqueous sol-gel method using [Emim][Tf_2N]	rutile nanorods, phase-directing properties of IL, removal of IL is key issue	[205]
	$Ti(OBu)_4$ in [C_4mim][PF_6] and MeOH	hollow microspheres, stirring rate and temperature as control parameters, IL as solvent and stabilizer	[214]
ZnO	zinc acetate and TBAH with aging at room temperature	mesocrystals consisting of nanoscale rod-like particles, number of particles decreases with duration	[201a]
	zinc acetate and TBAH with reflux at 100 °C	mesocrystals with complex morphology on a solid support	[201b]
	IL-ZnO composite	metal incorporated into IL as solvent and metal precursor, luminescent nanocrystals	[202]
	IL-Zn composite $Zn(H_2N\text{-}C_4H_9)_4^{2+}(Tf_2N^-)_2$	metal-containing IL precursor, spherical particles consisting of nanoplates and flower-like shapes, morphology strongly depends on Zn-IL type	[203]
	oleic acid, ethylenediamine and zinc acetate in a heating reaction	pyramidal morphology, ions in the mixtures of OA and organic amines play a key role in the formation of pyramids terminated by polar surfaces	[200]
	hydrothermal method	different ILs afford flower- and rod-like morphologies, IL as controller and inhibitor for agglomeration	[204]
SnO_2	sol-gel synthesis using [C_{16}mim][Br]	room temperature "green" reaction, wormhole-like pores, recyclable IL, gas sensing properties	[215]
	self-prepared L_{16} (hexadecyl-2-pyridinyl-methylamine) as IL in aging reaction	very high BET; optical, electrical, and dielectric properties at room temperature	[216]
CeO_2	solvent evaporation by heating in humidity oven using [C_4mim][Br]	spherical particles consisting of 3.5 nm nanocrystals with high BET, higher IL contents degrade structures into open worm-like mesopores	[218]
CuO	ultrasound-assisted synthesis using [C_4mim][Tf_2N] at room temperature	nanorods, high BET, widened band gap	[219]
Cu, Zn, and Fe-oxides; $CoFe_2O_4$ and $NiFe_2O_4$	TBAH at 100 °C and reflux	γ-Fe_2O_3/Fe_3O_4 cubes and spheres, CuO plates, EPR and magnetic behavior of $CoFe_2O_4$ and $NiFe_2O_4$	[209]
$InVO_4$	different temperatures and reaction times by using [Bmim][BF_4]	nanorods; IL as solvent, structure-directing and reducing agent; photoluminescence study	[220]
$LiFePO_4$	heating to 250 °C using several ILs	IL is recovered, application in Li-ion batteries	[210]
V_2O_5, VO_2	hydrothermal synthesis from IL-vanadium oxide nanocomposite	IL: (C_2mimBF_4); (C_4mimSO_3CF_3); (C_4mimBF_4) or (C_8mimBF_4), V_2O_5 nanocomposites and VO_2 nanosheets, IL intercalates into V_2O_5 crystal structure	[208]
V_2O_5	sol-gel synthesis with acetone and isopropanol using ([$Py_{1,4}$][Tf_2N]) and ([Emim][TF_2N])	cation type of the IL and type of organic solvent influence crystallinity, morphology and surface area of the mesoporous particles	[217]
YVO_4:Eu(@YF_3)	heating at 200 °C using [N(Me)(Bu)$_3$][$N(SO_2CF_3)_2$]	core-shell structures with nonluminescent shells to enhance luminescent properties	[211]

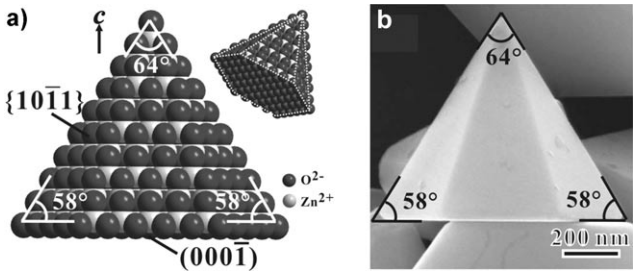

Figure 10. ZnO nanopyramids formed from an ionic-liquid-assisted approach: a) schematic growth model, b) representative SEM image of the products.[200] Reproduced with permission from The Royal Society of Chemistry.

The strong interaction of the IL with the oxide precursor can also result in a permanent intercalation as has been observed for the synthesis of lamellar nanostructured V_2O_5 in the presence of various ionic liquids ([C_2mim][BF_4], [C_4mim]-[SO_3CF_3], [C_4mim][BF_4], or [C_8mim][BF_4]).[208] According to WAXS/SAXS (wide angle X-ray scattering/small angle X-ray scattering) studies, a hybrid nanocomposite is formed by chemisorption of the IL along the [100] face so that the crystal growth process is selectively stopped. Therefore, ILs should be used with caution in the synthesis of nanomaterials with layered structures that are prone to such intercalation processes. The V_2O_5-IL composites were subjected to thermal post-treatment to afford V_2O_5 (5 h at 550 °C) or V_2O_3 (3 h at 700 °C), respectively.[208]

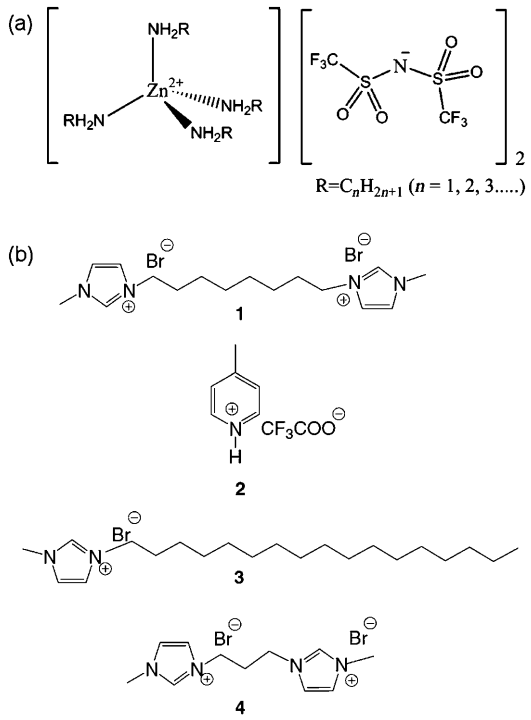

Scheme 1. a) Metal-containing IL precursor for the straightforward synthesis of ZnO nanoparticles[203] and b) different ILs screened for the formation of ZnO nanoparticles with various morphologies.[204] Copyright, Springer Verlag, 2010. Reprinted with permission.

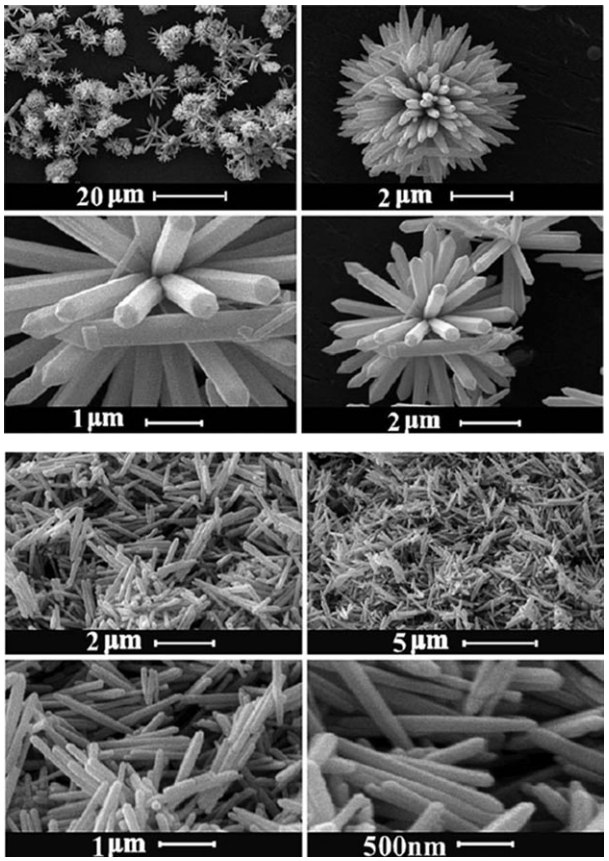

Figure 11. SEM images of the ZnO particles obtained in the presence of IL **1** (top four images) and IL **2** (bottom four images, for structures of ILs, see Scheme 1).[204] Copyright, Springer Verlag, 2010. Reprinted with permission.

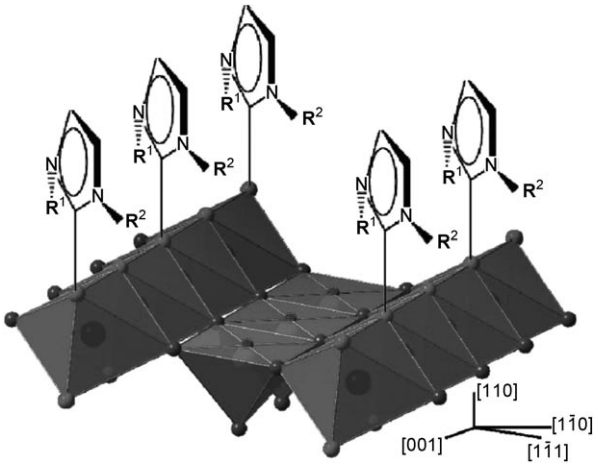

Figure 12. Model for the structure-directing influence of ionic liquids in the formation of rutile nanoparticles. Reprinted from Ref. [206], with permission. Copyright 2010 American Chemical Society.

As well as facilitating the synthesis many other binary nanostructured oxides, (e.g. CuO, ZnO, γ-Fe_2O_3/Fe_3O_4, Mn_3O_4, and several lanthanoid hydroxides, also see Table 5), ILs also give access to ternary oxides, namely the spinels $CoFe_2O_4$ and $NiFe_2O_4$.[209] Aqueous metal solutions were added to pre-heated TBAH (100 °C) and the reaction mixture was heated under reflux for 10 h. This rather straightforward method is a quick access to a variety of nanoscale shapes, such as cubic and spherical morphologies of γ-Fe_2O_3/Fe_3O_4, nanoplatelets of CuO, Mn_3O_4, and needle-like copper- or cobalt-doped ZnO. The ternary spinel oxides $CoFe_2O_4$ and $NiFe_2O_4$ were obtained from co-precipitation of the metal acetates with TBAH and these as-synthesized nanoparticular ferrites showed different magnetic behavior: the cobalt ferrite particles (11 nm) are ferromagnetic up to 400 K, whereas the smaller nickel ferrite particles (8 nm) exhibit superparamagnetism with a blocking temperature of 23 K. The $NiFe_2O_4$ particles meet the size criterion for the onset of superparamagnetism (particle sizes below 10 nm) and their properties are confirmed by the absence of temperature dependence in the EPR spectra between 100 and 273 K, contrary to the behavior of larger $CoFe_2O_4$ particles.[209]

$LiFePO_4$ is another oxide-based material with tremendous application potential in battery technology. Different nanoscale morphologies of $LiFePO_4$ could be obtained through an elegant approach based on the dual function of ILs as solvents and growth templates.[210] A variety of ILs were investigated with respect to the variation of the anionic component (e.g. $TFSI^-$, BF_4^-, $CF_3SO_3^-$, $C(CN)_3^-$, and Cl^-), the charge on the cationic centers (imidazolium, pyrrolidinium, and pyridinium), and the chain lengths (C2–C18) connected to the imidazolium cations, with special emphasis on the resulting physico-chemical characteristics of the ILs. Needle-shaped particles of $LiFePO_4$ were obtained by modifying the polarity of the medium through introduction of CN^- groups into the

$[Emim]^+$ cation, while platelets were formed in the presence of less-polar ILs with longer aliphatic chains. Interestingly, with the IL route, $LiFePO_4$ could not be obtained at temperatures below 200 °C in contrast to low-temperature solvothermal routes. This difference is probably due to the low solubility of the precursors in the ILs compared to other solvents and this effect must be considered when planning IL-based routes.[210]

Europium-doped yttrium vanadates are well-established red emitting phosphors that find widespread application in displays and fluorescent lamps. Nanocrystalline YVO_4:Eu and YVO_4:Eu@YF_3 are now available as monodispersed and redispersible particles from an elegant IL-assisted route in the presence of $[N(Me)(Bu)_3][N(SO_2CF_3)_2]$.[211] The addition of ethanol as a cosolvent to the reaction reduced the viscosity of the IL and enhanced the solubility of the precursors. Thermal post-treatment at 200 °C led to the formation of crystalline nanoparticles. Generally, preparing luminescent core–shell nanoparticles with a sufficient lattice matching between both components is an excellent strategy towards enhanced quantum yields. In the present case, the (001) lattice fringes of YVO_4 correlate well with the (100) fringes of YF_3, thereby leading to an increase in quantum yield from 17–19 % to 44–46 %.[211]

In summary, ILs are attracting more and more attention as versatile media for the synthesis of oxide-based and other nanomaterials. However, their strong structure-directing features may easily turn into a problem when the products contain unwanted IL residues. Although this may require further optimization work for setting up "green" and economic industrial processes, the advantages of ILs definitely outweigh their disadvantages as demonstrated in the following Section on combined synthetic methods.

2.5. Combined Synthetic Approaches

Although all of the synthetic strategies covered in the previous Sections provide an entire methodological arsenal in their own right, the current trends in the synthesis of nanomaterials definitely point to their combination into "synergistic" approaches as innovative routes to nanomaterials. These cutting-edge preparative endeavors are briefly highlighted and rounded off with an outlook on the future of advanced materials preparation. It is, however, noteworthy that a lot of fundamental work on the mechanistic principles behind each particular technique still lies ahead, as will be demonstrated in Section 3. Nevertheless, the mere inspiration of pushing the boundaries of oxide nanomaterials fabrication is an exciting endeavour in its own right.

2.5.1. Microwave-Assisted Synthesis in Combination with Ionic Liquids (MW-IL Approaches)

Ionic liquids (ILs) do not only act as highly efficient capping agents in the synthesis of nanomaterials, but they are also absorbents for microwave radiation. This makes combined MW-IL syntheses a particularly versatile option as illustrated for our example oxides ZnO, TiO_2, and SnO_2.

Zinc nitrate is transformed into nanostructured ZnO under microwave irradiation in the ionic liquid $[Bmim][BF_4]$.[104] The morphology of the products could be varied between flower-like particles in the presence of lower IL fractions and needle-like shapes upon increasing the IL content. The formation of ZnO needles could alternatively be steered through increasing the reaction temperature from 90 °C to 125 °C.

The high degree of phase and morphology control in MW-IL processes is illustrated by the synthesis of anatase nanocubes from the interaction of titanium isopropoxide with the ionic liquid $[Bmim][BF_4]$ under microwave irradiation.[112] In this case, the IL plays a multiple role as a microwave absorbent and a protecting agent for intermediates and anatase nanocubes. The size of the nanocubes was tuned through the reaction time and the water content of the system and a formation mechanism involving polyanions protected by $[Bmim]^+$ cations was proposed on the basis of FTIR, Raman, and HRTEM studies on isolated intermediates.

SnO_2 as another key binary oxide material has been accessed as microspheres through the MW-IL-assisted self-assembly of small tin oxide nanoparticles.[122] The anionic part of the ILs ($[Bmim][BF_4]$, $[Bmim][PF_6]$, $[Omim][BF_4]$, $[Bpy][BF_4]$, [Bmim][Cl]) interacts with the surface of the growing SnO_2 nuclei so that the surface energy is minimized through the formation of spherical structures. The microwave treatment clearly influences this process by speeding up the nucleation so that the resulting spherical aggregates are massive in contrast to their hollow counterparts obtained from conventional heating. Prolonged reaction times favor the breakup of the initial multisphere junctions and their recrystallization into less-polydisperse microspheres.

Furthermore, the IL-based synthesis of luminescent nanooxides can be enhanced through microwave methods, as demonstrated for the fast and efficient approach to $LaPO_4$:Ce,Tb nanoparticles from a mixture of the metal chlorides in the presence of $[MeBu_3N][(SO_2CF_3)_2N]$.[221] Remarkably, neither an inorganic surface shell nor a coordinating surface modifier is required to produce luminescent particles with a high quantum yield after complete removal of the IL. This is an impressive example of the technological potential of combined MW-IL approaches.

2.5.2. Ionic Liquids in Ultrasonic Synthesis

In analogy to MW-IL methods, the combination of ILs with ultrasound-assisted syntheses is another promising development in the synthesis of oxide nanoparticles. Recently, ZnO nanorods were obtained from the reaction of zinc acetate in the presence of the ionic liquid $[C_4mim][Tf_2N]$ after ultrasonication of the reaction mixture in a sealed glass tube at room temperature.[222] CuO nanorods (30–100 nm in length, 10 nm in diameter) were furthermore prepared from an analogous synthetic method.[219] This effective template- and surfactant-free approach is therefore expected to bring forward a wide spectrum of oxide nanomaterials.

Further examples for combined synthetic approaches to nanostructured oxides are summarized in Table 6 and this

Table 6: Combined synthetic routes to nanostructured oxides (examples are sorted in alphabetical order).

Oxide	Technique	Morphology/features	Ref.
CuO	MW-IL using [Bmim][BF_4]	leaf-, chrysanthemum- and rod-like shapes with varying IL concentration	[104]
	MW-IL using [Omim][TA]	flower- and leaf-like structures with varying IL concentration	[222]
	US-IL using [C_4mim][TF_2N]	rod-like shapes (30-100 nm in length and 10 nm in diameter)	[112]
SnO_2	MW-HT-IL using different ILs	small irregular nanoparticles with self-assembly into microspheres	[223]
TiO_2	MW-IL using [Bmim][BF_4]	bipyramid-shaped anatase with pseudo cube-like appearance	[224]
ZnO	MW-IL	flower- (more water) and needle-like (more IL) shapes	[219]
	US-IL using [C_4mim][Tf_2N]	rod-like shape (50–100 nm length range) and 20 nm diameter	[122]
Other oxides			
FeOOH, α-Fe_2O_3	MW-IL using [Bmim][BF_4]	hollow spheres in μm range for FeOOH, spherical α-Fe_2O_3 particles (ca. 20 nm) synthesized without IL	[221]
$LaPO_4$:Ce,Tb	MW-IL using [$MeBu_3N$]-[$(SO_2CF_3)_2N$]	spherical to slightly ellipsoidal particles with sizes of 9–12 nm	[225]
$La_{0.8}Sr_{0.2}Co_{0.5}Fe_{0.5}O_{3\pm\delta}$	MW + sol-gel using [Bmim]-[BF_4]	perovskite structure with spherical morphology	[226]
$PbCrO_4$, Pb_2CrO_5	MW-IL using [Bmim][BF_4]	with NaOH: bundle- and rod-like Pb_2CrO_5; without NaOH: $PbCrO_4$ rods	[227]

survey is only the "tip of a preparative iceberg" that will grow over the coming years.

3. In Situ Methods for Investigating the Mechanism of Oxide Nanomaterials Formation

3.1. Scope and Trends of In Situ Investigations

The previous Sections gave an overview of recent progress in the synthesis of oxide nanomaterials, demonstrating that an impressive preparative arsenal is now available to access nanostructured oxides in a wide variety of phases and morphologies and to fine-tune the particle surfaces. Nevertheless, the limited number of ternary and higher nano-oxides remains a challenging problem: most of the above-mentioned methods still do not offer a generally applicable design approach towards oxide nanomaterials. Although considerable progress has been achieved in the general understanding of nucleation and crystal growth processes in solution,[228,229] they still remain elusive for many oxide materials so that the prediction of the crystal structure resulting from a specific reaction is frequently difficult. This situation may render the subsequent step of morphology control in nanomaterials fabrication complicated, if not entirely impossible. However, crystal-shape engineering is a topic of general and vital industrial interest that affects all aspects of a product from processing through to surface properties and on to handling and storage.[230] Although the success in nanoscale oxides synthesis has been impressive over the last years, it has frequently been achieved through empirical strategies, such as "trial and error" and the lateral transfer of the resulting insights to analogous reaction systems. As a result, there is a growing urgency to understand the nucleation and growth processes in oxide nanomaterials formation on a more substantial level and on a wider scale. The ultimate goal of such endeavors is the targeting and design of oxide nanomaterials with the strategic efficiency and versatility of organic chemistry or inorganic coordination chemistry.

In the following, we focus on solution-based in situ techniques that are applicable to a wide spectrum of the above-mentioned synthetic pathways and that require either generally available synchrotron facilities or even more-common laboratory analytically techniques. Furthermore, these in situ strategies permit the observation of bulk nanoparticle formation processes for significant reaction volumes, thereby affording insights that are vital for their industrial scale-up.

It should be kept in mind that microscopy techniques emerge as very sophisticated tools to monitor crystallization kinetics and growth mechanisms.[231,232] In situ NMR spectroscopy has, for example, also proven highly efficient to elucidate the nucleation and growth of nano- and mesoporous inorganic solids.[233] However, the signal sensitivity and spectral resolution of NMR spectra are highly dependent upon the natural abundance of the isotope under investigation. This situation makes in situ NMR spectroscopy an excellent method to investigate the nucleation and growth process of zeolites containing Si or/and Al.[233] On the other hand, it also means that the general application potential of in situ NMR spectroscopy for multi-element systems remains limited. Therefore, the present discussion is concentrated on solid-state diffraction techniques and spectroscopic methods in solution, so as to cover a maximum range of synthetic approaches to nanomaterials.

As illustrated in the previous Section, many nanostructured oxides are prepared under special non-ambient conditions using closed and nontransparent vessels so that the direct kinetic monitoring of these systems is a difficult task. Although basic kinetic information can also be obtained from quenching experiments and their ex situ analyses, these indirect strategies always bear the risk of isolating artifacts that might falsify further conclusions on the reaction mechanism. Therefore, the continuous in situ monitoring of nanomaterials formation is the most detailed and accurate approach and it also provides information about intermediate phases occurring during the reaction process. Hence, the direct monitoring strategies are also the technically most demanding options. The penetration of the reaction vessel walls with high-intensity radiation is particularly efficient and has been reviewed in great detail.[234] For this purpose, the high flux of X-rays from a synchrotron source is most suitable

Table 7: Survey of oxide nanomaterials formation processes studied with in situ methods (oxides are listed in alphabetical order and from binary to higher oxides).

Oxide	In situ method	Feature	Ref.
Fe_2O_3	SAXS/WAXS	kinetics and mechanisms of Fe_2O_3 nanoparticle formation	[248]
MnO_2	XRD	hydrothermal crystallization of β-MnO_2 nanorods	[246]
MnO_2	XRD	in situ characterization of phase transformations	[247]
MoO_3	EDXRD/XAS	formation pathway of MoO_3 fibers	[250]
TiO_2	SAXS/WAXS	growth kinetics of TiO_2 nanoparticles	[236]
TiO_2	IR	molecular kinetics and particle formation of TiO_2 nanocrystals	[237]
TiO_2	XRD	hydrothermal crystallization of TiO_2 nanoparticles	[238]
TiO_2	IR	self-assembly pathway of TiO_2 nanofibers	[239]
ZnO	SAXS	growth mechanism of ZnO nanorods	[240, 241]
ZnO	in situ grazing-incidence diffraction	formation of ZnO nanoparticles during the early stages of the growth process	[242]
ZnO	UV/Vis/NMR/Raman/XAS	nucleation and growth of ZnO in various organic solvents	[243]
ZnO	SAXS/UV/Vis	growth kinetics of ZnO nanocrystals	[244, 245, 282]
ZrO_2	XRD	crystallization mechanism of monoclinic ZrO_2 nanocrystals	[249]
ZrO_2, TiO_2, SiO_2	ATR-FTIR	reaction kinetics	[239]
Multimetal systems			
Bi_2MoO_6	EDXRD	reaction kinetics of Bi_2MoO_6 nanosheet formation	[252]
Bi_2MoO_6	XRD/XAS/Raman	phase formations/transformations in the initial reaction stages	[253]
$CoAl_2O_4$	QEXAFS/XRD	formation mechanism of nanosized $CoAl_2O_4$ spinel particles	[254]
M_xWO_3	EDXRD/XAS	reaction kinetics of M_xWO_3 nano-oxide formation	[63]
$M_x(W/Mo)O_3$	EDXRD	reaction kinetics of $M_x(W/Mo)O_3$ nano-oxide formation	[84, 251]

in terms of intensity, time resolution (far below the minute scale), and accuracy.[235]

A survey of recent research activities concerning the mechanistic in situ investigation of nanoscale oxide synthesis is provided in Table 7. In line with the synthetic trends, the majority of the in situ studies are focused on binary oxides with wide applicability and high commercial relevance, namely ZnO and TiO_2. However, the rapid development of synthetic methods and their application to the formation of a wide range of oxide nanomaterials can only be systemized and fully exploited through a tremendous amplification of the present mechanistic knowledge. In other words, a wide gap is opening up between the ever growing number of synthetic methods and the in-depth analysis of their underlying formation pathways—especially in the case of ternary and higher oxides which have the most promising potential for new properties. Needless to say, the required in situ investigations quickly turn into analytical challenges, but tackling them is the key to tailoring oxide materials directly for the demands of modern nanotechnology—from tuned properties to facile industrial production processes.

The third Section of this Review therefore outlines the most recent efforts to monitor the nucleation and growth processes of nanoscale oxides in real time with advanced radiation sources and experimental setups. Selected results demonstrate the tremendous power of in situ methods to elucidate the different stages of nanomaterials formation processes.

3.2. In Situ Powder Diffraction Techniques

To date, diffraction techniques have been widely used to track the kinetics, growth steps, and phase changes of solid-state syntheses through the time-dependent evolution of diffraction patterns.[255–259] As high intensities and time resolutions (timescale of seconds) are indispensable for in situ studies, these studies are mostly performed with position-sensitive detectors and polychromatic radiation. In the course of these energy-dispersive X-ray diffraction (EDXRD) techniques, data are collected with a fixed-angle solid-state photon-counting and energy-discriminating detector and the Bragg diffraction is recorded as a function of the energy instead of the commonly used diffraction angle. The high-intensity polychromatic radiation can even penetrate a stainless steel hydrothermal cell without substantial intensity loss, thus facilitating the experimental setups considerably. In situ EDXRD techniques can be applied to monitor dynamic processes in a wide variety of compound types and one of the most impressive examples is the observation of "breathing" processes in metal–organic frameworks (MOFs) during the intercalation of organic guest molecules. These findings shed important light on the application of MOFs for storage, sensor, and separation technologies.[260] The high efficiency of in situ EDXRD techniques in the kinetic analysis of more complex oxide systems is illustrated in the following for selected examples.

Nanoscale tungsten oxides are promising materials and their wide variety of structural motifs provides many options for nanomaterials fabrication. Some of us have performed in situ EDXRD investigations of the hydrothermal growth kinetics of nanoscale hexagonal tungsten oxides in the presence of alkali halides as morphology-directing additives.[63] Although the different alkali cations bring forward a wide range of hexagonal tungstate morphologies, all these processes have a nucleation-controlled mechanism in common. However, the hydrothermal synthesis of nanostructured hexagonal W/Mo-oxides[84,251] by the same hydrothermal strategy displayed a strong dependence of both the formation mechanisms and the particle morphologies on the

alkali halide auxiliaries. Interestingly, a kinetically based correlation between the type of alkali cation additive, the reaction mechanism, and the emerging morphology could be established: whereas hierarchically structured spherical architectures are formed by the same diffusion mechanism in the presence of the heavier alkali chlorides (K, Rb, Cs), the mechanistic influence of Li^+ and Na^+ ions is more complicated.

The BIMOVOx oxide family in general[261] is noteworthy as a result of these oxides' interesting structural and materials properties that attract considerable research attention as illustrated by their most recent high-throughput synthesis.[262] Their tungsten-containing counterparts are equally promising sources for new nanomaterials with advanced catalytic features. Bi_2WO_6, for example, is an important visible-light-driven photocatalyst and several groups have reported synthetic pathways to hierarchically constructed Bi_2WO_6 microspheres consisting of individual nanoparticles. Initially, polymer additives, such as polyvinyl pyrrolidone (PVP), were considered indispensable for the formation of such hierarchical nanoscale arrangements.[79,263,266] However, Bi_2WO_6 spheres can also be obtained in the absence of any templating polymers and the initial pH value of the hydrothermal system was identified as the crucial factor for steering phase and morphology of the emerging products.[80,264,267,268] The wide parameter window for the preparation of Bi_2WO_6 microspheres inspired us to perform further in situ EDXRD studies on their template-free hydrothermal formation. Given that the above-mentioned hierarchically grown M-W/Mo-oxides (M = K, Rb, Cs) all have a three-dimensional diffusion-controlled growth model in common (as shown by the reaction exponent $m = 0.55$),[251] mechanistic investigations on hierarchical Bi_2WO_6 microspheres are of interest to discover trends in the formation of self-organized architectures. Therefore, we monitored the hydrothermal synthesis of Bi_2WO_6 through in situ EDXRD experiments with special emphasis on the reaction temperature and the initial pH value. A typical in situ EDXRD pattern is shown in Figure 13 and the growth rates and kinetic models were determined according to the standard literature methods.[269] We found that an increase of the synthesis temperature reduced both the onset time and the half-life time of the crystallization process. Nevertheless, the growth profiles did not vary significantly with temperature, thereby demonstrating that the growth mechanism of Bi_2WO_6 particles is not temperature-dependent in the interval from 150 to 170 °C. Furthermore, the corresponding reaction exponents varied between 0.52 and 0.55: this is in good agreement with the three-dimensional diffusion-controlled growth model that is also applicable for the formation of hierarchically structured spherical W/Mo-oxide particles.[84,251] Therefore, diffusion-controlled mechanisms are clearly a common denominator for the self-organization of nanosized building blocks into microspheres in chemically different hydrothermal systems. An initial increase in pH value does not only decrease the onset and half-life time of the crystallization process of Bi_2WO_6 microspheres, but it also influences the reaction exponent: a shift in pH value from 1.3 to 4 changes the reaction exponent from 0.52 to 0.7. As a consequence, the three-dimensional diffusion-controlled growth model is not applicable at pH values around 4, and the mechanistic change is morphologically reflected in a disintegration of the Bi_2WO_6 microspheres into the individual nanoplate building blocks. In situ EDXRD studies are thus a powerful tool to track morphology–kinetics relationships and to single out their most influential reaction parameters.

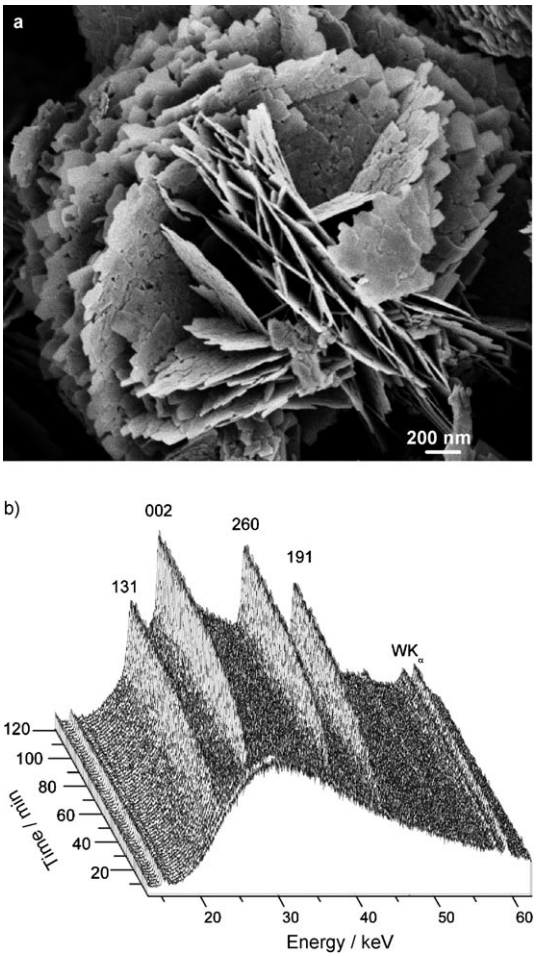

Figure 13. a) Representative SEM image of hierarchical Bi_2WO_6 microspheres, b) a time-resolved energy-dispersive X-ray powder diffraction pattern of their formation.

Regarding the technically important bismuth molybdates, a comprehensive in situ EDXRD study was performed to investigate the hydrothermal formation kinetics of their representatives with the highest catalytic activities, namely α-$Bi_2Mo_3O_{12}$, β-Bi_2MoO_9, and γ-Bi_2MoO_6.[252] As a result, both α-$Bi_2Mo_3O_{12}$ and γ-Bi_2MoO_6 were found to emerge directly from the amorphous gel mixture without any intermediates involved. Furthermore, the reaction kinetics of γ-Bi_2MoO_6 nanosheet formation were correlated with the structure and morphology of the material in terms of a 2D diffusion-controlled model.

Despite their widespread and successful application, the poor angular resolution of the position-sensitive detectors is an inherent drawback of EDXRD methods. This renders the extraction of detailed information about the crystal structure and particle size often impossible, so that the required high-

quality data need to be obtained from in situ synchrotron X-ray diffraction.

In situ high-resolution powder diffraction (HRPD) therefore provided a more detailed insight into the above-mentioned crystallization kinetics of Bi_2MoO_6 in combination with XAS (X-ray absorption spectroscopy) and Raman techniques.[253] The presence of isolated MoO_4^{2-} ions in the initial stages of the reaction was confirmed through XANES (X-ray absorption near edge structure) and Raman investigations and the following reaction pathway was proposed on the basis of refined HRPD data (Figure 14a): Firstly, a Bi_2O_3-related intermediate with a distorted fluorite structure is formed. These particles are converted into the layered Aurivillius-type structure of Bi_2MoO_6 upon prolonged reaction times.

In situ HRPD investigations can also shed new light on well-established crystallization models, as demonstrated in a recent study on the high-temperature, high-pressure formation of ZrO_2 nanoparticles from gels.[249] Generally, monoclinic ZrO_2 has been known as the thermodynamically stable bulk phase, whereas the metastable tetragonal ZrO_2 is stabilized in nanoparticles below a critical size limit of 30 nm as a result of the lower surface energy. However, for the gels under investigation, the local structure of did not bear a resemblance to any of these established modifications and they were subsequently transformed into monoclinic ZrO_2 particles with diameters of only few nanometers. The conventional surface energy-stabilization model for free particles fails to explain these experimental results and there is clearly no lower size limit for monoclinic ZrO_2 nanocrystals.

Advanced in situ XRD studies furthermore reveal more subtle phase transitions that are not accompanied by any morphological changes, as has recently been demonstrated for the hydrothermal formation of β-MnO_2 nanorods.[246] The first step is a dissolution–recrystallization process leading to γ-MnO_2 nanorods as an intermediate. These undergo an isotopological short-range rearrangement of MnO_6 octahedra to yield β-MnO_2 nanorods as the final product. Another representative example is the understanding of the dehydroxylation pathway from nanosized $In(OH)_3$ to bixbyite-type In_2O_3 through in situ time-resolved synchrotron radiation so that InOOH could definitely be ruled out as an intermediate phase.[270]

3.3. In Situ X-ray Absorption Spectroscopy

Although in situ X-ray diffraction techniques often are the "method of choice" to investigate the formation kinetics of nanostructured oxides, they do not permit the direct observation of particles smaller than approximately 5 nm, as these fall below the detection limits of Bragg diffraction methods. Consequently, these techniques are not equipped to monitor the decisive nucleation stages during the measured induction periods. Moreover, rearrangements in liquid and amorphous phases are not detectable either, so complementary X-ray absorption spectroscopy (XAS) methods are required to obtain insight into the short-range order of materials.[271] As XAS techniques provide information about

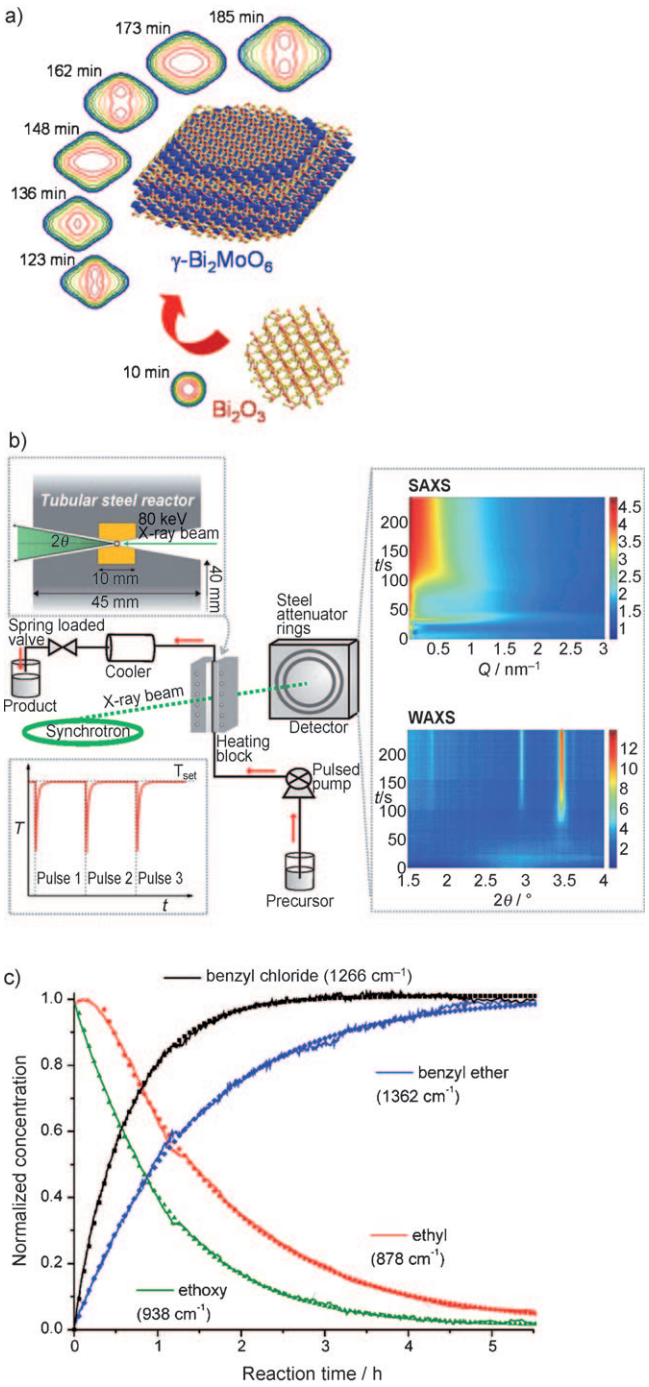

Figure 14. a) Crystallization mechanism proposed for the growth of γ-Bi_2MoO_6 under hydrothermal conditions.[253] Reproduced with permission from The Royal Society of Chemistry. b) Experimental setup for SAXS and WAXS in situ studies.[248] c) Normalized kinetics of benzyl chloride and benzyl ether formation and of the reaction of ethoxy- and ethyl-containing species in the growth of TiO_2 nanoparticles from non-aqueous media.[237] Reproduced with permission of The Royal Society of Chemistry.

the coordination environment and oxidation state of the absorber, regardless of its degree of crystallinity, their combination with in situ X-ray diffraction is a very far-reaching and comprehensive strategy. Furthermore, the reaction pathways of nanomaterials within matrices, for

example, the reduction of Fe_2O_3 nanoparticles in amorphous carbon, can be clearly traced with in situ XAS.[272]

The efficiency of such combined in situ approaches has been demonstrated by some of us for the hydrothermal transformation of $MoO_3 \cdot 2H_2O$ into MoO_3 fibers.[250] As the educts and products bear close structural resemblance, a topotactic transformation would have been quite a reasonable reaction mechanism. However, in situ XAS studies of both the liquid and solid phase during the conversion process, in combination with in situ EDXRD measurements, showed that the MoO_3 rods are formed by a quick dissolution–precipitation mechanism—contrary to "chemical intuition". The products precipitate within a few minutes, a process in which neither residual starting material nor intermediates play a role.

However, the acquisition of high quality data for EXAFS (extended X-ray absorption fine structure) investigations with a high time resolution remains a difficult task. Most often, only the XANES (X-ray absorption near edge structure) data are used to investigate the local environment and the oxidation state of the absorber. Thus, in situ XAS investigations should be combined with at least one backup technique to reconstruct a given reaction process with a sound model.

A brief case study from our work on the formation of new $Bi_6S_2O_{15}$ nanowires[273] may illustrate that in situ XAS is often indispensable to get to the bottom of gradual transformations of bulk precursors into nanomaterials that do not proceed by quick and straightforward pathways, such as dissolution–nucleation–recrystallization sequences. New $Bi_6S_2O_{15}$ nanowires are formed from the direct hydrothermal reaction of commercially available Bi_2O_3 in highly concentrated K_2SO_4 solutions. Firstly, the induction time of the reaction was estimated from ex situ quenching experiments to be around 5 min. Next, in situ EDXRD measurements did not point to any structural changes or to dissolution of the Bi_2O_3 precursor, thereby suggesting a solid–solid transformation as the most plausible mechanism. To acquire more detailed insight into the liquid phase of the hydrothermal system, we performed in situ QEXAFS (quick-scanning extended X-ray absorption spectroscopy) investigations[274] at the Bi-L_3 edge. They indicated a solubility of approximately 0.4 mol% Bi at 160 °C, thereby pointing to a slower reaction process. Indeed, the in situ EDXRD results had created a misleading image of the reaction sequence and kinetics, because the products observed during the very first stages of the nanowire formation are in fact bulk Bi_2O_3 particles overgrown with a thin layer of $Bi_6S_2O_{15}$ nanowires. Unfortunately, the reflections of the overgrown particles are concealed by the much stronger scattering power of the residual Bi_2O_3 precursor. In addition, the strongest diffraction peak of the $Bi_6S_2O_{15}$ phase overlaps with the much stronger (012) reflection of Bi_2O_3, thereby rendering standard in situ X-ray diffraction techniques entirely inappropriate in the present case. Two models can now be proposed for the formation of $Bi_6S_2O_{15}$ nanowires: The first option is a homogeneous solution-phase reaction between dissolved Bi^{3+} and SO_4^{2-} ions (slow dissolution–recrystallization mechanism). Another mechanistic option is the heterogeneous transformation involving solid Bi_2O_3 and soluble SO_4^{2-} ions. As our in situ QEXAFS studies show only a slight dissolution of Bi_2O_3 under the given hydrothermal conditions, they strongly support the dissolution–recrystallization route.

3.4. In Situ Small-Angle X-ray Scattering (SAXS)

Small-angle X-ray scattering (SAXS) permits the size evaluation of small particles up to around 100 nm through the analysis of the scattering intensity of X-rays over a small angular range from approximately 0.1° to 3°.[275–277] In addition, SAXS is also suitable for the analysis of amorphous materials. The information obtained about particle size, shape, and size distribution is crucial for elucidating the nucleation processes of nanomaterials and furthermore is complementary to the above-mentioned powder diffraction or wide-angle X-ray scattering (WAXS) techniques.

In situ SAXS/WAXS is therefore a powerful experimental combination, as has been demonstrated by the investigation of the formation of TiO_2 nanoparticles in supercritical fluids.[236] The supercritical sol–gel process offers the considerable advantages of low reaction temperature (100 °C) and a fast time scale (ca. 50 min) compared to the corresponding conventional strategy. This approach thus opens up new avenues to the efficient fabrication of high-quality nanomaterials[278] within minutes rather than hours. Another representative example for the efficient combination of complementary in situ SAXS and WAXS techniques is the monitoring of a fast (in minutes) and environmentally friendly hydrothermal process leading to magnetite (Fe_2O_3) nanoparticles (see setup in Figure 14b).[248] According to in situ SAXS data, an amorphous phase is formed only 40 s prior to crystallization. These amorphous cluster intermediates decompose quantitatively and give way to magnetite nanocrystals.

As outlined in detail in the previous Sections of this Review, ZnO nanoparticles are among the most important oxide tools for modern nanotechnology. Therefore, understanding the nucleation and crystallization processes of ZnO nanoparticles is vital for optimizing their materials properties and the synthetic routes for commercial purposes.[241] This goal has been frequently pursued with the help of in situ UV/Vis absorption spectroscopy (see below), but in situ SAXS approaches are more suitable for investigating the mechanistic influence of the capping agents that are employed to control the morphology of the emerging ZnO nanocrystals. For example, kinetic in situ SAXS studies on the growth of ZnO nanorods in the presence or absence of PVP as a capping agent clearly demonstrate the mechanistic impact of the organic additive: the ZnO nanorod growth follows a diffusion-limited Ostwald ripening mechanism in the absence of PVP, whereas the PVP-assisted growth mechanism is more complex and data fits suggest that both diffusion and surface reactions play an important role.[240]

Layered hydroxides (LHs) are closely related to oxide nanomaterials and they can be further transformed into nanostructures by intercalation processes.[279] As these compounds represent a new class of multifunctional materials with oxide building blocks, detailed insights into their

formation kinetics in solution are also relevant for related oxide nanoparticles syntheses. The recent investigation of anion-exchange reactions of layered α-cobalt hydroxides is a representative example for the efficient combination of in situ SAXS/WAXS with in situ EDXRD techniques.[257,280] Interestingly, different host compounds, $Co(OH)_{1.75}(DDS)_{0.25}\cdot 0.6\,H_2O$ and $Co(OH)_{1.7}Cl_{0.3}\cdot 0.4\,H_2O$ (DDS = dodecylsulfate), vary with respect to the extent of carbonate exchange and the resulting stacking, whereas the exchange reaction kinetics of both follow a two-dimensional diffusion controlled model.

3.5. In Situ Spectroscopy (IR, Raman, and UV/Vis)

In principle, the growth of nanoparticles can also be monitored through in situ vibrational spectroscopy, especially with IR and Raman methods. Although these strategies might at first glance be favorable from a practical point of view, the spectra obtained are often difficult to interpret with conventional evaluation methods owing to pronounced peak overlaps. Furthermore, spectroscopic methods frequently require the use of organic solvents so that their application window is considerably narrowed. Nevertheless, the following examples demonstrate that in situ spectroscopy can prove highly efficient in the investigation of selected synthetic processes, such as nanoparticles formation in non-aqueous media.

The non-aqueous sol–gel synthesis of TiO_2 nanoparticles from $TiCl_4$ in the presence of benzyl alcohol and ethanol was tracked with in situ FTIR spectroscopy to correlate the transformation of the organic reagents with the TiO_2 particle growth (Figure 14c).[237] The observed reaction kinetics for the formation of TiO_2 nanoparticles from benzyl alcohol reveals that benzyl chloride and benzyl ether are formed as organic side products and that the corresponding consumption of ethyl- and ethoxy species could be fitted to first-order kinetics. As a result, two parallel mechanisms with different kinetics, namely alkyl halide elimination and ether elimination, could be assigned and their roles in the formation of TiO_2 nanoparticles were discussed.

As the optical properties of nanoparticles strongly depend on their size, the crystallization of spherical particles can be studied with in situ UV/Vis methods through monitoring the change in absorption edges.[281] This indirect approach correlates the absorption edge to the particle size, thereby providing reliable data on the average size and size distribution of the growing nanocrystal assembly. However, the method is strictly limited to spherical particles and it is therefore not suitable for materials with anisotropic features.

Once more, examples for unusual insights obtained with the help of in situ UV/Vis spectroscopy can be found in the field of ZnO synthesis.[244,282] Interestingly, in situ UV/Vis studies on the formation of ZnO nanoparticles from zinc acetate and NaOH in isopropanol showed that the observed growth mechanism deviates from the widely accepted diffusion-controlled coarsening process (Ostwald ripening). Instead, an intermediate scenario between the two well-defined limits of diffusion control and kinetics control could be assigned and the capping role of Na^+ ions opens up further interesting perspectives for inherent morphology control through reactants.

Another multidisciplinary study employing UV/Vis, Raman, XAS, and ^1H NMR spectroscopy illustrates the various growth steps of ZnO nanocrystals from a special organometallic precursor in different organic solvents (Figure 15).[243] Three different regimes for nucleation and

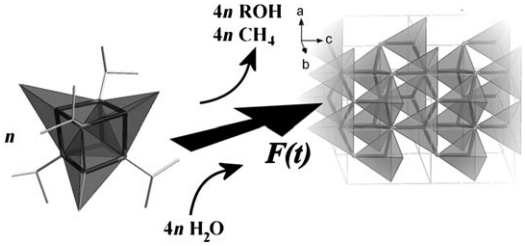

Figure 15. Selective formation of ZnO (wurtzite) from the reaction of the organometallic zinc oxo heterocubanes precursors with water. Reprinted from Ref. [243], with permission. Copyright 2010 American Chemical Society.

growth could be identified: in the nucleation-dominated regime, the solvent type is the most influential factor, whereas the particle growth is proportional to the precursor concentration in the growth-dominated regime. At very low precursor concentrations the growth of ZnO nanocrystals is again concentration dependent.

Note that the possibilities of in situ Raman spectroscopy using visible and IR wavelengths are usually limited through strong fluorescence interference that is caused by organic solvents, impurities, and surface defect sites. The recent development of UV Raman techniques is a promising approach to diminish the fluorescence-related interference and to enhance the signal intensity as well as the resulting sensitivity.[283] As the formation mechanism of microporous materials, such as AlPO-5[284] and zeolite X,[285] under hydrothermal conditions has been successfully investigated, in situ UV Raman is an up-coming powerful option to study the mechanisms of oxide nanomaterials formation.

Generally, the field of in situ investigations has grown rapidly over the past years and a large methodological arsenal is now available to monitor the growth kinetics and nucleation processes leading to the formation of nanomaterials. However, even this brief survey demonstrates clearly that the insight into the crystallization mechanisms of oxide nanomaterials is still limited to selected systems. As a consequence, further studies are required, especially on ternary and higher oxides which have a potential to be tuned for technological applications. From the technical point of view, there is still plenty of room for improving the time resolution of in situ methods. Furthermore, the combination of different monitoring techniques will certainly play a major role in future studies to obtain complementary insight into a reaction system and to shed light on the growth processes from different analytical angles. The selected examples demonstrate the tremendous potential of in situ methods to derive general trends for structure and morphology control on the nanoscale level. Finally, all these efforts towards a "nano-toolbox concept"

would be incomplete without the development of theoretical models for nucleation and growth processes in different reaction media. As this highly dynamic and interesting research area is beyond the scope of the present Review, we just want to conclude this part by directing the reader's attention towards the tremendous potential of synergies between experimental and theoretical studies on nanomaterials growth, for example, in the task of modeling nucleation processes in solution.[40,286–288]

4. Oxide Nanomaterials for Innovative Applications

After the survey of the synthetic and analytical aspects of nanostructured oxide materials in the previous Sections, we round off our Review by looking at their status in today's industrial developments. We have selected a few examples from different technological fields (catalysis, sensors, and data processing) that exemplify how tailoring oxide nanoparticles paves the way to hitherto unexplored properties and applications beyond the well-known macroscopic features. These examples illustrate how transforming oxides onto the nanoscale opens up new applications that are important in industry as well as in everyday life.

Although many useful nanotechnological strategies are based on the downsizing of macroscopic applications to nanoscale dimensions, the most exciting scope of nanotechnology is the discovery of fundamentally new properties in thin films, nanowires, or nanoparticles. Furthermore, on conversion into nanomaterials, many materials properties undergo a significant change below a critical size limit, these properties include mechanical plasticity,[289–291] phase-transition temperature,[292–295] electronic properties,[296,297] and magnetic behavior.[289,298] To date, these manifold empirical observations are explained with a limited number of concepts, such as the particle dimensions approaching the characteristic length scale of the property under consideration: this may be the minimal size of a dislocation loop for plasticity in metals or the domain size in ferroelectric and ferromagnetic materials. These effects can, for example, be impressively observed for the transition from ferromagnetic to superparamagnetic behavior in particles that are sufficiently small for thermal vibrations to overcome the energy gain from ferromagnetic ordering so that the uniform spin orientation is lost.[299]

Another established feature of nanomaterials is their large amount of surface atoms, which, for particles below 10 nm, can easily be increased to several tens of atom %.[300] The resulting structural rearrangements frequently give rise to a significantly enhanced reactivity of the material which can be described using a core–shell model with different properties for bulk and surface regions. A typical example of this kind of size effect is the reduction of the glass transition temperature in thin films of polymer glasses.[293]

4.1. Industrial Trends for the Production of Oxide Nanomaterials

Despite the tremendous progress in the development of elaborate nanomaterials over the past years, their large-scale industrial application and production are still mainly focused on a selection of commercially relevant "classics". In the previous Sections, ZnO, TiO_2, and SnO_2 were chosen as major "example oxides" to outline recent progress on the laboratory scale. The key market position of binary oxide nanomaterials is evident from a recent survey of companies dealing with nanomaterials in the UK.[301] The main markets are in the US (49 %) and in Europe (30 %) with TiO_2, iron and aluminum oxides being the leading nanomaterials in terms of the quantities manufactured. Another representative study on nano-toxicology identifies iron oxide, ZnO, TiO_2, and CeO_2 as the most important materials.[300] Whereas ZnO and TiO_2 nanoparticles find widespread applications in sunscreens and photocatalysts, nanoscale iron oxides are applied for separation purposes (see Section 4.2) and for pigment fabrication. Small CeO_2 nanoparticles (< 10 nm) are useful additives in Diesel fuels. In Switzerland, for example, these trends are reflected in the following annual production statistics for oxide nanomaterials in 2008: TiO_2 (435 t/a), iron oxide (365 t/a), aluminum oxide (100 t/a, particle sizes > 100 nm), SiO_2 (75 t/a), and ZnO (70 t/a).[302] Over the past years, the major industrial applications for nanoparticles in general remained in the areas of paints/coatings, cosmetics, catalysts, and polymer composites. Nanocomposites are frequently produced using nano-clay (the fraction of natural clay with particle sizes below 100 nm) as a cheap filler and additive for enhanced strength and resistance.[303] Concerning more specialized processes, quantum dots for authentication, magnetic storage media, and nanoporous batteries/sensors are in the focus of industrial interest.

In the following, we demonstrate how nanoscale effects offer new and convenient application concepts.

4.2. Magnetic Separation of Catalytic Nanoparticles

Despite the outstanding catalytic features of nanomaterials, their separation and regeneration from the products of a given reaction can turn into a major technical challenge, especially for the most reactive particles with dimensions lower than 10 nm. It goes without saying that the fixation of the nanoparticles on an inert carrier surface is not an efficient solution to this problem. Although the removal of nanoscale catalyst particles through filtration or centrifugation is a better option, both processes are too tedious for industrial production.[304]

The fast and selective separation of particles through magnetic separation is therefore being industrially implemented on a wide scale, ranging from ore refinement to the food industry (Figure 16a and b).[304]

As magnetic separation can only be applied on materials with appropriate ferromagnetism, many catalytically active nanoparticles have to be coupled with magnetic cores for this purpose. Furthermore, an unwanted influence of the magnetic material is often minimized through a core–shell approach. To

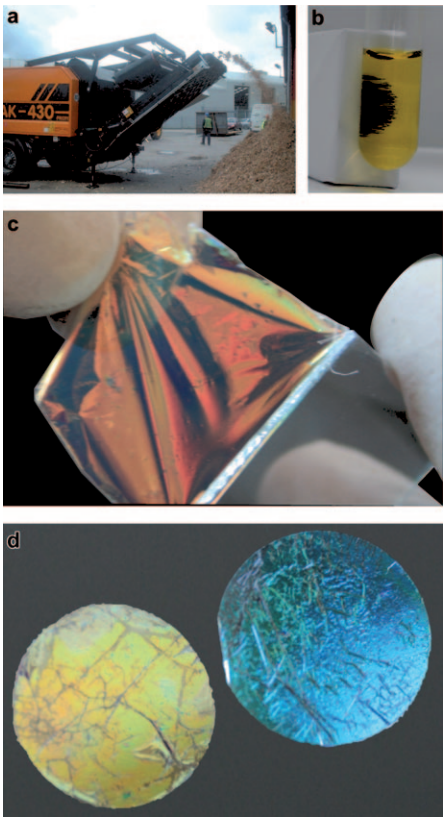

Figure 16. a) Image of an industrial-scale magnetic separator. The magnet is located in the box suspended above the conveyor belt; b) laboratory scale setup for magnetic separation (1.5 ml vessel); c) a polycarbonate-infiltrated Bragg stack can be peeled off its glass substrate and d) redeposited onto a Si wafer.[335] Reproduced with permission from The Royal Society of Chemistry.

minimize the side effects of particle growth and subsequent agglomeration into multicore particles, the materials can be functionalized with a stabilizing agent after synthesis (peptization). Despite the extensive use of magnetic separation in biotechnology,[305–307] the number of magnetically separable inorganic catalysts is still limited. One of the most straightforward examples is the use of magnetite (Fe_3O_4) nanocatalysts to catalyze the protection of hydroxy groups with trimethylsilyl (TMS) groups.[308]

Magnetite and maghemite (γ-Fe_2O_3) are easily accessible and inexpensive so that they are most widely used for core–shell approaches to magnetize other catalyst materials.[299] Although the higher saturation magnetization of magnetite makes it the material of choice at first glance, its rapid oxidation into maghemite is a drawback that may furthermore be difficult to detect with X-ray diffraction methods.[309,299] The direct contact of the catalyst material with the magnetic core can be avoided with a thin layer of amorphous silica or through coating with synthetic- and biopolymers as common practice in biotechnology.[306] For applications involving inorganic catalysts, though, there are many points which speak for amorphous silica as the separation material, for example, its easy deposition from solution with controlled layer thicknesses, the electrically insulating properties and the presence of hydrophilic silanol groups on the materials surface as anchors for further functionalization.[310–313] Although silica-coated magnetic cores can also facilitate the removal of homogeneous catalysts,[314] we focus on their use in heterogeneous catalysis in the following.

As mentioned above, the many applications of TiO_2 in white pigments (rutile modification) and as (photo)catalysts (preferably anatase modification) make it an oxide nanomaterial with key industrial significance.[315] After the direct combination of photocatalytic titania nanoparticles with magnetic iron oxide cores was unsuccessful due to mutual degradation,[316] the magnetic center was protected with amorphous silica layers.[317] Recently, the conventional sol–gel/calcination approach for the coupling of TiO_2 to the silica-coated magnetic cores was optimized in a very detailed study on the direct deposition of titanium dioxide on insulated magnetic nanoparticles.[317] Whereas the conventional sol–gel process yields multicore particles with a relatively low surface area, a significant increase of the water content in the reaction system led to the homogeneous nucleation of titania nanoparticles and to their subsequent heterocoagulation with the silica coated magnetite particles. This formation mechanism requires a careful adjustment of the pH value in the range between 3 and 4 to ensure that the particle types carry opposite charges (Figure 17). Although the as-synthesized

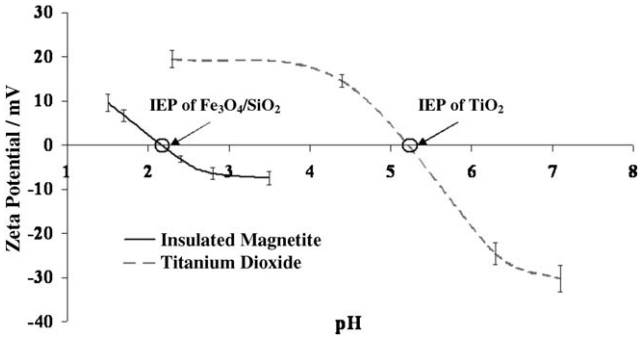

Figure 17. Zeta-potential as a function of pH value for silica-coated magnetite and titantia nanoparticles; the isoelectric points (IEPs) of the particles are highlighted.[317] Copyright, Springer Verlag, 2010. Reprinted with permission.

crystalline anatase nanoparticles already display a good adherence to the silica-coated magnetite particles, the composite formation could be further improved through calcination at 250 °C and above, with a negligible decrease of the specific surface area.

The major advantage of the heterocoagulation strategy in comparison with conventional routes is the resulting high surface area of the magnetically functionalized titania catalysts. This approach is expected to be applied to the preparation of other magnetically separable catalyst systems—provided that the following requirements can be fulfilled: a) a pH window of opposite surface charges of the catalyst and the silica particles has to be established and b) the composite particles should exhibit sufficient mechanical stability under post-treatment, that is, minimal losses of specific surface area. A two-step heterocoagulation process with separate syntheses of the catalyst particles and the

magnetic nanocores, followed by mixing at a suitable pH value would certainly provide access to a variety of magnetically separable heterogeneous nanocatalysts. Representative examples of such catalysts are listed in Table 8.

Next, we switch from synthetic to analytic applications of nanoscale oxides and we have selected the interdisciplinary field of photonic crystals for this purpose.

Table 8: Core–shell nanoparticles for magnetically separable catalysts.

Catalytic material	Special features	Ref.
Fe_3O_4	catalyzes the protection of hydroxy groups with TMS	[308]
Fe_3O_4@SiO_2	linked to a Ru-complex catalyst	[314]
Fe_3O_4@TiO_2	photodegradation of core observed	[316]
Fe_3O_4@SiO_2@TiO_2	effect of precursor concentration, time and temperature investigated	[317]
$NiFe_2O_4$@SiO_2@TiO_2	reverse micelle technique	[318]
Fe_3O_4@SiO_2@SiO_2:Ti	used for H_2O_2-based selective oxidations	[309]
Fe_2O_3@SiO_2@Au	gold NPs electrostatically attached, conversion of CO into CO_2 tested	[319]

4.3. Inorganic Nanoparticles for One-Dimensional Photonic Crystals

Photonic crystals are periodic arrays of light-scattering entities with a periodicity in the order of magnitude of the radiation wavelength under consideration. One-dimensional photonic crystals, also known as Bragg stacks or thin optical filters, are constructed from periodic stacks of thin films of two materials with different refractive indices.[320,321] A part of each wave travelling from one material to the other is reflected with the ratio of reflectance to transmittance depending on the difference in refractive indices. Each 1D photonic crystal has a characteristic photonic band gap that prevents the passing of specific wavelengths so that they are reflected instead (for a more detailed description of this phenomenon see Refs. [320,321]). The wavelength of maximal reflectivity λ_{max} depends on the layer-thickness of the stack [Eq. (1)]

$$\lambda_{max} = 2(n_l d_l + n_h d_h) \quad (1)$$

where n is the refractive index and d the layer thickness of the material with higher (h) and lower (l) refractive index, respectively. Note that Equation (1) is only valid for light waves perpendicular to the stack. When the angle of incidence is inclined, λ_{max} is usually shifted to larger wavelengths as illustrated in Figure 18. The fraction of light with a given wavelength that is actually reflected R furthermore depends on the refractive index difference with the refractive index of the substrate n_s and the number of layers N in the stack [Eq. (2)].[320]

$$R = \left(\frac{1-Y}{1+Y}\right)^2 \quad \text{with } Y = \left(\frac{n_h}{n_l}\right)^{N-1}\frac{n_h^2}{n_s} \quad (2)$$

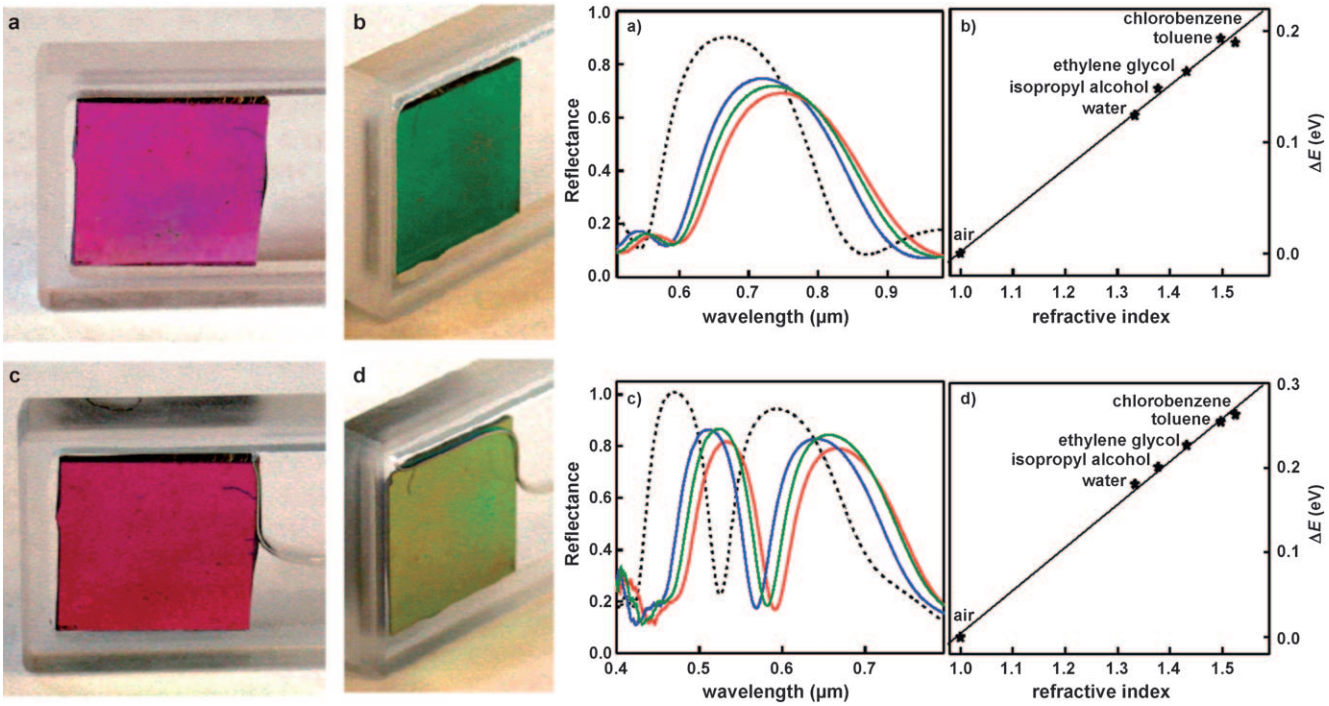

Figure 18. Left: a) and b) Bragg reflector with four double layers of TiO_2 and SiO_2 nanoparticles in air; c) and d) the same Bragg reflector immersed in ethanol; note the angular dependency of the wavelength of maximal reflection.[323] Right: a), b) Optical response of a Bragg reflector with eight double layers of SiO_2 and TiO_2 nanoparticles in air (dotted line), water (blue), ethylene glycol (green), and chlorobenzene (red); c), d) show a Bragg reflector with an optical defect (one of the SiO_2 layers in the middle of the stack is thicker than the others) that allows a more accurate determination of the peak position.[324] Reprinted from Refs. [323, 324], with permission. Copyright 2010 American Chemical Society.

As the opacity of powders and colloids is due to light being scattered by the particles, they become transparent when the particle sizes are considerably smaller than the wavelength of the incident light. These principles also apply for porous thin films with according particle size dimensions so that they can be treated as homogeneous materials with an effective refractive index.[322]

The advantage of porous Bragg stacks is that the wavelength of maximal reflection of the stack depends on the refractive index of the pore content. This feature can be used for sensor applications: for example, the wavelength shift of organic solvents can be distinguished with Bragg stacks consisting of less than ten layers of SiO_2 and TiO_2 nanoparticles (Figure 18, left; see also Table 9)[323,324] as has recently been demonstrated for the correlation of the wavelength shift to the partial pressure of toluene.[325] The sensitivity of this sensor type can be furthermore enhanced by "doping" the stack with a thicker layer to create allowed states in the optical band gap that lead to a sharp indentation within the broad reflection peak (Figure 18, right).[324,326]

Table 9: Porous Bragg stacks for sensing applications.

Components	Remarks	Ref.
TiO_2 and SiO_2	sensor for organic solvents within the pores	[323–325]
TiO_2 (different particle sizes)	Bragg stacks from a single material	[329]
SiO_2, TiO_2, SnO_2, SnO_2:Sb	construction of semiconducting Bragg stacks	[327]
TiO_2 (different particle sizes)	increase of the efficiency of Grätzel cells using a porous Bragg stack	[328]
TiO_2 and SiO_2	surface fictionalization of pores for more specific sensing	[336]
TiO_2 and poly-HEMA	swelling of poly-HEMA is used for very sensitive water sensors	[330]
polymer infiltrated stacks	Flexible Bragg reflectors	[332–335]

TiO_2 and SiO_2 are a perfect match for Bragg stacks owing to their pronounced difference in refractive indices, as are other oxide combinations: the replacement of the insulator SiO_2 with pure or antimony-doped tin oxide (Sb:SnO_2, ATO) would open up the opportunity to create photoconductive Bragg stacks that could, for example, enhance the efficiency of dye-sensitized solar cells.[326–328] However, porous Bragg stacks often do not even require the use of two different materials, because the periodic modulation of the refractive index can alternatively be achieved through an according modulation of the pore size.[329]

The application potential of Bragg stacks as well as their options for advanced functionalization can be amplified in combination with organic molecules and polymers. The swelling of the organic layers in hybrid Bragg stacks can thus precisely indicate even minimum amounts of solvent vapor while the inorganic layer serves as a high refractive index material, as has been recently demonstrated for a Bragg stack with TiO_2 and poly-HEMA (poly(hydroxyethylmethacryl acid) layers.[330] Likewise, the introduction of magnetic cores within flexible polymeric shells would allow the interlayer distance of such Bragg stacks to be influenced with magnetic fields.[331] Finally, flexible Bragg reflectors can be constructed by infiltrating the pores of nanoparticular Bragg stacks with polymers. The resulting nanocomposite reflectors can be applied to mechanically strained substrates that cannot be combined with the inherently brittle ceramic thin-film Bragg reflectors.[332–335] This approach was recently demonstrated for polycarbonate-infiltrated nanostructured Bragg reflectors: they can even be lifted off their substrate and be reapplied to a different surface (Figure 16c and d).[335]

In summary, nanoparticle based one-dimensional photonic crystals provide the exciting option to translate changes of the chemical environment within their pores into an easily readable optical signal with tunable wavelength. Even though transparent materials are an indispensable requirement for the preparation of Bragg mirrors, the wide arsenal for their construction, namely the many combinations of oxide and other inorganic nanoparticles, polymers, and functionalized surfaces, opens up almost endless possibilities. The resulting devices can be used as sensors for gases and compounds in solution, for dye-sensitized solar cells, or as easily applicable Bragg mirrors for decoration.

Finally, we conclude this brief insight into the technological potential of oxide nanomaterials with an outlook on their key role in the developing field of nano-magnetic applications.

4.4. Magnetic Behavior of Oxidic Nanostructures

Over the past years, diluted magnetic semiconductors (DMS) have attracted increasing research interest owing to their high application potential in spintronics ("spin-transport electronics"). The concept of spintronics is expected to revolutionize data processing and light-emitting diode (LED) technology and to bring forward ultra-fast optical switches.

The most basic option to generate a spin-polarized current is to pass a current through a ferromagnetic medium, for example, to create a giant magnetoresistance (GMR) device,[337–339] and complex oxide materials (such as, manganites, double perovskites, spinel ferrites) offer an exceptionally rich spectrum of electronic properties that can be widely tuned for applications in the field of spintronics.[340] In principle, electrical spin injection can also be evoked by passing a current through a metallic ferromagnet, but the large impedance mismatch between ferromagnetic materials and semiconductors renders the injection across metal-semiconductor interfaces rather inefficient. As intrinsically magnetic semiconductors are only applicable at temperatures well below ambient conditions to date,[341,342] the doping of classic semiconductor materials was proposed as a strategy to combine the properties of both materials types into dilute magnetic semiconductors (DMSs) with Curie temperatures (T_c) above room temperature.[343]

This effect has, for example, been reported for the doping of TiO_2 with approximately 7 atom% Co, and other oxides (e.g. ZnO or SnO_2) were transformed into diluted magnetic semiconductors through doping with Co or Mn, and even undoped oxides have been reported to show the desired properties.[344] However, these findings have to be handled with great care, because their reproducibility and their theoretical background are still being controversially discussed.[344–347] From the practical point of view, these doping processes are extremely prone to artifacts, such as minimal contaminations that may be unintentionally picked up during the preparation (such as, dust or particles from tweezers or pigments in marker-inks).[344,348]

The ongoing debate about high T_c ZnO-based DMSs[349] illustrates the "important difference between a *magnetic semiconductor* and a *semiconductor that is magnetic*".[350] As outlined in a recent critical Review, several methodological pitfalls readily lead to the latter scenario so that the observed magnetic behavior may in fact arise from magnetic secondary-phase formation when the solid solubility limit of the dopant is exceeded.[350] Defect formation then leads to impurity band formation above some percolation threshold. Correlated substitution effects also have to be carefully ruled out, because they can significantly reduce the average moment per dopant atom through mutual spin-vector cancellation in antiferromagnetic pairs.[350] Conventional powder-diffraction techniques are incapable of detecting these subtle effects so that a sophisticated combination of high-resolution XRD and XAS techniques is indispensable to ensure the quality of DMS materials. X-ray linear dichroism (XLD), namely XANES investigations with linearly polarized X-rays, furthermore helps to track the detailed environment of dopant ions as has been shown for cobalt-doped ZnO epitaxial films that turned out to be paramagnetic.[350] To prevent the formation of secondary ferromagnetic phases, copper has been proposed as the ideal dopant for inducing room-temperature ferromagnetism (RTFM) in ZnO.[349] In the course of a recent study on RTFM in copper-doped ZnO nanowires synthesized by chemical vapor deposition, the ferromagnetic ordering of the as-grown samples was ascribed to extrinsic sources (CuO nanoparticles) as well as intrinsic ones ($Zn_{1-x}Cu_xO$ nanowires) and their influences on the net ferromagnetism were differentiated through follow-up annealing experiments in Zn vapor and Zn/O_2 vapor, respectively.[351]

A different strategy towards interface-related magnetism has recently been developed for ZnO nanoparticles that were covered with a self-assembled monolayer (SAM) of dodecanethiol or dodecylamine.[352] The ferromagnetism-related properties of the composites are explained with a charge-transfer mechanism from ZnO to the organic molecules and similar phenomena have been reported for thiolated SAMs on gold surfaces.[353,354]

These examples illustrate the emergence of new oxide properties on the nanoscale and it will be interesting to investigate whether this charge-transfer magnetic effect can be expanded to a wide spectrum of substrate materials, including semiconductors (e.g. Si, Ge, GaAs…) and other oxide materials. If so, the replacement of the organic SAMs with thermally and mechanically robust inorganic coatings would be desirable to generate extremely thin magnetic layers and nanoparticles for future nano-magnetic technologies.

5. Summary and Outlook

Although this Review of recent developments in the synthesis and application of oxide nanomaterials can only tentatively sketch the dimensions of this vast research field, it is clear that the initial question raised in the introduction can be answered in a positive manner: over the past rich and intense "Seven Fat Years", we have witnessed tremendous synthetic, methodological, and technological progress in oxide nanomaterials, with no limits in sight. Compared to the 1990s, most of the manifold individual studies on nanoscale oxides are now multidisciplinary and application-oriented and the general trend is moving from fundamental preparative explorations to in-depth studies that are focused on straightforward production strategies and on future technical implementations.

On the synthetic front, the classic solution-based techniques, such as sol–gel and hydrothermal methods, have become more and more differentiated and this preparative repertoire for nano-oxides is now being enriched with innovative approaches, such as microwave and ultrasound techniques. In the coming years, these new individual strategies might thus be combined into hybrid tailored approaches that can be used to selectively prepare technologically important complex nanoscale oxides with the individually adapted techniques (MW, US, HT, IL techniques, …) serving as preparative building blocks.

At present, most preparative activities are still directed at the commercially relevant binary oxide nanomaterials, such as TiO_2, ZnO, SiO_2, and iron oxides, but the art of complex nanomaterials synthesis has already paved the way to multicomponent oxide nanocatalysts and to the phase- and morphology-selective preparation of ternary oxide nanomaterials (e.g. nanostructured spinels, garnets, and perovskites). Whereas template-directed nanomaterials synthesis has been greatly emphasized during the pioneering years of the field, templates are currently more and more replaced with "smart solvents", such as ionic liquids and physico-chemical strategies of morphology control: the potential of cavitation and "hot spot" phenomena occurring in ultrasound- and microwave-assisted processes is just beginning to be explored in depth.

Consequently, it has become difficult to keep track of all these dynamic developments on the mechanistic level. However, insights into the nucleation and growth processes of nanomaterials are indispensable to navigate a reaction system through the "Bermuda triangle" of phase, composition, and morphology control towards the desired nanostructured oxide. This task becomes increasingly difficult when two or more cations have to be organized into a single nanomaterial, not to mention the further options for anionic substitutions to generate, for example, oxyhalides or oxynitrides. Fortunately, the arsenal of in situ methods for mechanistic studies has also been expanded continuously over the past decade so that the

accuracy and efficiency of the key in situ diffraction techniques now permits the monitoring of important ternary oxide formation processes in real time. In this way, the influence of templates and reaction parameters on the phase and morphology of the resulting oxide materials is being clarified for a growing number of examples, so that the first trends for general synthetic strategies appear on the horizon. Highly specialized in situ XAS and SAXS/WAXS techniques furthermore deliver key information about the onset and timescale of nucleation processes and the subsequent interplay between different product phases has been modeled for many processes on the basis of high-quality data. Hopefully, these developments will widen the preparative "bottleneck" of morphology control in ternary oxide materials.

Most importantly, the insights from in situ techniques need to be exploited for the large-scale industrial production of oxide nanomaterials, for which, synthetic robustness, efficiency, and reliability are indispensable criteria that can be profoundly met with mechanistic knowledge.

The new applications of oxide nanomaterials, for example, in magnetically separable catalysts or optical gas sensors, require the most precise control of the deposition, precipitation, and coagulation mechanisms. Only joint preparative, mechanistic, and theoretical efforts can fully convert current technologies down to the nano level. In principle, chemists are now methodologically well equipped to make oxide nanotechnology work for the urgent and world-wide issues of the 21st century, especially the depletion of energy and water sources. Intense interdisciplinary efforts will be required to systemize the vast amount of empirical knowledge into general and clear-cut guidelines for the rapid and flexible design of new nanomaterials. Oxide nanomaterials are a fascinating and multifaceted research area that keeps attracting scientists and they bear a great responsibility to come up with solutions for the problems of our next decades, such as water splitting for hydrogen-based energy technologies, the large-scale photocatalytic recycling of waste water, miniaturized energy storage and harvesting of all kinds, or personalized nanosensors for the detection of increasing health and atmospheric hazards. In short, future research on functional oxides should be committed to address the needs of our ever growing society.

This work was supported by the Swiss National Science Foundation (SNSF Professorship PP002-114711/1) and by the University of Zurich. The support of the Electron Microscopy ETH Zurich, EMEZ, and of the Center for Microscopy and Image Analysis, University of Zurich, is gratefully acknowledged. We wish to thank Prof. Dr. Jan-Dierk Grunwaldt (Karlsruhe Institute of Technology (KIT)) for his generous support with in situ XAS studies and Prof. Dr. Wolfgang Bensch (University of Kiel, Germany) for the fruitful collaboration on in situ EDXRD investigations.

Received: January 14, 2010
Published online: November 25, 2010

[1] a) G. A. Ozin, L. Cademartiri, *Small* **2009**, *5*, 1240; b) G. A. Ozin, L. Cademartiri, *Concepts of Nanochemistry*, Wiley-VCH, Weinheim, **2009**.
[2] C. N. R. Rao, A. Müller, A. K. Cheetham, *The Chemistry of Nanomaterials*, Wiley-VCH, Weinheim, **2004**.
[3] J. A. Rodriguez, M. Fernandez-Garcia, *Synthesis, Properties, and Applications of Oxide Nanomaterials*, Wiley InterScience, New York, **2007**.
[4] Y. E. Gogotsi, *Nanomaterials Handbook*, CRC, Taylor & Francis, Boca Raton, **2006**.
[5] G. A. Ozin, A. C. Arsenault, *Nanochemistry: A Chemical Approach to Nanomaterials*, RSC Publishing, London, **2005**.
[6] a) D. Vollath, *Nanomaterials*, Wiley-VCH, New York, **2008**; b) H. Goesmann, C. Feldmann, *Angew. Chem.* **2010**, *122*, 1402; *Angew. Chem. Int. Ed.* **2010**, *49*, 1362.
[7] G. R. Patzke, F. Krumeich, R. Nesper, *Angew. Chem.* **2002**, *114*, 2554; *Angew. Chem. Int. Ed.* **2002**, *41*, 2446.
[8] S. T. Bromley, I. D. R. Moreira, K. M. Neyman, F. Illas, *Chem. Soc. Rev.* **2009**, *38*, 2657.
[9] C. S. S. R. E. Kumar, *Nanomaterials for the Life Sciences*, Wiley-VCH, Weinheim, **2010**.
[10] W. H. Suh, Y. H. Suh, G. D. Stucky, *Nano Today* **2009**, *4*, 27.
[11] J. S. Murday, R. W. Siegel, J. Stein, J. F. Wright, *Nanomed. Nanotechnol. Biol. Med.* **2009**, *5*, 251.
[12] J. H. Gao, H. W. Gu, B. Xu, *Acc. Chem. Res.* **2009**, *42*, 1097.
[13] Y. W. Chun, T. J. Webster, *Ann. Biomed. Eng.* **2009**, *37*, 2034.
[14] K. E. Lundin, O. E. Simonson, P. M. D. Moreno, E. M. Zaghloul, I. I. Oprea, M. G. Svahn, C. I. E. Smith, *Genetica* **2009**, *137*, 47.
[15] N. Sozer, J. L. Kokini, *Trends Biotechnol.* **2009**, *27*, 82.
[16] V. Mailänder, K. Landfester, *Biomacromolecules* **2009**, *10*, 2379.
[17] N. R. Shiju, V. V. Guliants, *Appl. Catal. A* **2009**, *356*, 1.
[18] R. Bogue, *Sens. Rev.* **2009**, *29*, 310.
[19] M. Zach, C. Hagglund, D. Chakarov, B. Kasemo, *Curr. Opin. Solid State Mater. Sci.* **2006**, *10*, 132.
[20] T. Pradeep, Anshup, *Thin Solid Films* **2009**, *517*, 6441.
[21] A. Weidenkaff, R. Robert, M. H. Aguirre, L. Bocher, L. Schlapbach, *Phys. Status Solidi RRL* **2007**, *1*, 247.
[22] F. Hernandez-Ramirez, J. D. Prades, R. Jimenez-Diaz, T. Fischer, A. Romano-Rodriguez, S. Mathur, J. R. Morante, *Phys. Chem. Chem. Phys.* **2009**, *11*, 7105.
[23] J. Garcia-Barriocanal, A. Rivera-Calzada, M. Varela, Z. Sefrioui, M. R. Diaz-Guillen, K. J. Moreno, J. A. Diaz-Guillen, E. Lborra, A. F. Fuentes, S. J. Pennycook, C. Leon, J. Santamaria, *ChemPhysChem* **2009**, *10*, 1003.
[24] B. L. Cushing, V. L. Kolesnichenko, C. J. O'Connor, *Chem. Rev.* **2004**, *104*, 3893.
[25] X. Wang, Y. D. Li, *Inorg. Chem.* **2006**, *45*, 7522.
[26] W. T. Yao, S. H. Yu, *Int. J. Nanotechnol.* **2007**, *4*, 129.
[27] K. Byrappa, T. Adschiri, *Prog. Cryst. Growth Charact. Mater.* **2007**, *53*, 117.
[28] W. J. Crookes-Goodson, J. M. Slocik, R. R. Naik, *Chem. Soc. Rev.* **2008**, *37*, 2403.
[29] N. Krumov, I. Perner-Nochta, S. Oder, V. Gotchev, A. Angelov, C. Posten, *Chem. Eng. Technol.* **2009**, *32*, 1026.
[30] N. Ma, E. H. Sargent, S. O. Kelley, *J. Mater. Chem.* **2008**, *18*, 954.
[31] S. S. Behrens, *J. Mater. Chem.* **2008**, *18*, 3788.
[32] M. G. Blamire, J. L. MacManus-Driscoll, N. D. Mathur, Z. H. Barber, *Adv. Mater.* **2009**, *21*, 3827.
[33] M. Osada, T. Sasaki, *J. Mater. Chem.* **2009**, *19*, 2503.
[34] Z. G. Yang, D. Choi, S. Kerisit, K. M. Rosso, D. H. Wang, J. Zhang, G. Graff, J. Liu, *J. Power Sources* **2009**, *192*, 588.
[35] P. Nalawade, B. Aware, V. J. Kadam, R. S. Hirlekar, *J. Sci. Ind. Res.* **2009**, *68*, 267.

[36] A. Ghicov, P. Schmuki, *Chem. Commun.* **2009**, 2791.
[37] R. J. Gorte, J. M. Vohs, *Curr. Opin. Colloid Interface Sci.* **2009**, *14*, 236.
[38] R. Tenne, G. Seifert, *Annu. Rev. Mater. Res.* **2009**, *39*, 387.
[39] W. Y. Kim, Y. C. Choi, S. K. Min, Y. Cho, K. S. Kim, *Chem. Soc. Rev.* **2009**, *38*, 2319.
[40] a) S. M. Woodley, R. Catlow, *Nat. Mater.* **2008**, *7*, 937; b) M. S. Islam, P. R. Slater, *MRS Bull.* **2009**, *34*, 935.
[41] C. N. R. Rao, B. Raveau, *Transition Metal Oxides*, 2nd ed., Wiley-VCH, Weinheim, **1998**.
[42] A. Müller, P. Kögerler, A. W. M. Dress, *Coord. Chem. Rev.* **2001**, *222*, 193.
[43] A. Müller, F. Peters, M. T. Pope, D. Gatteschi, *Chem. Rev.* **1998**, *98*, 239.
[44] G. Kickelbick, *J. Sol-Gel Sci. Technol.* **2008**, *46*, 281.
[45] G. Férey, *Chem. Soc. Rev.* **2008**, *37*, 191.
[46] a) A. K. Cheetham, C. N. R. Rao, *Science* **2007**, *318*, 58; b) A. J. Bailey, C. Lee, R. K. Feller, J. B. Orton, C. Mellot-Draznieks, B. Slater, W. T. A. Harrison, P. Simoncic, A. Navrotsky, M. C. Grossel, A. K. Cheetham, *Angew. Chem.* **2008**, *120*, 8762; *Angew. Chem. Int. Ed.* **2008**, *47*, 8634.
[47] R. J. Kuppler, D. J. Timmons, Q. R. Fang, J. R. Li, T. A. Makal, M. D. Young, D. Q. Yuan, D. Zhao, W. J. Zhuang, H. C. Zhou, *Coord. Chem. Rev.* **2009**, *253*, 3042.
[48] C. N. R. Rao, A. K. Cheetham, A. Thirumurugan, *J. Phys. Condens. Matter* **2008**, *20*, 083202.
[49] G. Frenzer, W. F. Maier, *Annu. Rev. Mater. Res.* **2006**, *36*, 281.
[50] M. Jansen, *Angew. Chem.* **2002**, *114*, 3896; *Angew. Chem. Int. Ed.* **2002**, *41*, 3746.
[51] P. Bowen, C. Carry, *Powder Technol.* **2002**, *128*, 248.
[52] a) K. An, T. Hyeon, *Nano Today* **2009**, *4*, 359; b) D. Kim, J. Park, K. An, N.-K. Yang, J.-G. Park, T. Hyeon, *J. Am. Chem. Soc.* **2007**, *129*, 5812; c) R. Strobel, A. Baiker, S. E. Pratsinis, *Adv. Powder Technol.* **2006**, *17*, 457.
[53] K. C. Patil, S. T. Aruna, S. Ekambaram, *Curr. Opin. Solid State Mater. Sci.* **1997**, *2*, 158.
[54] I. Marozau, A. Shkabko, G. Dinescu, M. Dobeli, T. Lippert, D. Logvinovich, M. Mallepell, C. W. Schneider, A. Weidenkaff, A. Wokaun, *Appl. Surf. Sci.* **2009**, *255*, 5252.
[55] M. Yoshimura, K. Byrappa, *J. Mater. Sci.* **2008**, *43*, 2085.
[56] K. Byrappa, M. Yoshimura, *Handbook of Hydrothermal Technologies*, William Andrew, New Jersey, **2001**.
[57] R. E. Riman, W. L. Suchanek, M. M. Lencka, *Ann. Chim. Sci. Mater.* **2002**, *27*, 15.
[58] Y. Mao, T. J. Park, F. Zhang, H. Zhou, S. S. Wong, *Small* **2007**, *3*, 1122.
[59] A. Cabanas, J. A. Darr, E. Lester, M. Poliakoff, *Chem. Commun.* **2000**, 901.
[60] I. Djerdj, D. Arcon, Z. Jaglicic, M. Niederberger, *J. Solid State Chem.* **2008**, *181*, 1571.
[61] P. Horcajada, S. Surble, C. Serre, D. Y. Hong, Y. K. Seo, J. S. Chang, J. M. Greneche, I. Margiolaki, G. Ferey, *Chem. Commun.* **2007**, 2820.
[62] M. M. Titirici, M. Antonietti, A. Thomas, *Chem. Mater.* **2006**, *18*, 3808.
[63] A. Michailovski, R. Kiebach, W. Bensch, J. D. Grunwaldt, A. Baiker, S. Komarneni, G. R. Patzke, *Chem. Mater.* **2007**, *19*, 185.
[64] C. J. Jia, L. D. Sun, F. Luo, X. D. Han, L. J. Heyderman, Z. G. Yan, C. H. Yan, K. Zheng, Z. Zhang, M. Takano, N. Hayashi, M. Eltschka, M. Klaui, U. Rudiger, T. Kasama, L. Cervera-Gontard, R. E. Dunin-Borkowski, G. Tzvetkov, J. Raabe, *J. Am. Chem. Soc.* **2008**, *130*, 16968.
[65] T. Zhang, C. G. Jin, T. Qian, X. L. Lu, J. M. Bai, X. G. Li, *J. Mater. Chem.* **2004**, *14*, 2787.
[66] J. F. Lu, Y. Hakuta, H. Hayashi, T. Ohashi, T. Nagase, Y. Hoshi, K. Sato, M. Nishioka, T. Inoue, S. Hamakawa, *J. Supercrit. Fluids* **2008**, *46*, 77.
[67] J. H. In, H. C. Lee, M. J. Yoon, K. K. Lee, J. W. Lee, C. H. Lee, *J. Supercrit. Fluids* **2007**, *40*, 389.
[68] A. Celaya Sanfiz, T. W. Hansen, F. Girgsdies, O. Timpe, E. Rödel, T. Ressler, A. Trunschke, R. Schlögl, *Top. Catal.* **2008**, *50*, 19.
[69] H. M. Xiao, S. Y. Fu, L. P. Zhu, Y. Q. Li, G. Yang, *Eur. J. Inorg. Chem.* **2007**, 1966.
[70] S. B. Wang, Y. L. Min, S. H. Yu, *J. Phys. Chem. C* **2007**, *111*, 3551.
[71] G. R. Patzke, A. Michailovski, F. Krumeich, R. Nesper, J. D. Grunwaldt, A. Baiker, *Chem. Mater.* **2004**, *16*, 1126.
[72] B. Nagappa, G. T. Chandrappa, J. Livage, *Pramana* **2005**, *65*, 917.
[73] H. Uchiyama, H. Ohgi, H. Imai, *Cryst. Growth Des.* **2006**, *6*, 2186.
[74] B. Cheng, J. M. Russell, W. S. Shi, L. Zhang, E. T. Samulski, *J. Am. Chem. Soc.* **2004**, *126*, 5972.
[75] R. Menzel, A. M. Peiro, J. R. Durrant, M. S. P. Shaffer, *Chem. Mater.* **2006**, *18*, 6059.
[76] D. Reyes-Coronado, G. Rodriguez-Gattorno, M. E. Espinosa-Pesqueira, C. Cab, R. de Coss, G. Oskam, *Nanotechnology* **2008**, *19*, 145605.
[77] G. T. Chandrappa, N. Steunou, S. Cassaignon, C. Bauvais, J. Livage, *Catal. Today* **2003**, *78*, 85.
[78] G. Clavel, M. G. Willinger, D. Zitoun, N. Pinna, *Adv. Funct. Mater.* **2007**, *17*, 3159.
[79] L. S. Zhang, W. Z. Wang, L. Zhou, H. L. Xu, *Small* **2007**, *3*, 1618.
[80] Y. Zhou, K. Vuille, A. Heel, G. R. Patzke, *Z. Anorg. Allg. Chem.* **2009**, *635*, 1848.
[81] L. N. Sun, Q. R. Guo, X. L. Wu, S. J. Luo, W. L. Pan, K. L. Huang, J. F. Lu, L. Ren, M. H. Cao, C. W. Hu, *J. Phys. Chem. C* **2007**, *111*, 532.
[82] S. H. Lee, T. W. Kim, D. H. Park, J. H. Choy, S. J. Hwang, N. Z. Jiang, S. E. Park, Y. H. Lee, *Chem. Mater.* **2007**, *19*, 5010.
[83] Y. M. Hu, H. S. Gu, Z. L. Hu, W. N. Di, Y. Yuan, J. You, W. Q. Cao, Y. Wang, H. L. W. Chan, *Cryst. Growth Des.* **2008**, *8*, 832.
[84] R. Kiebach, N. Pienack, W. Bensch, J. D. Grunwaldt, A. Michailovski, A. Baiker, T. Fox, Y. Zhou, G. R. Patzke, *Chem. Mater.* **2008**, *20*, 3022.
[85] A. Michailovski, M. Wörle, D. Sheptyakov, G. R. Patzke, *J. Mater. Res.* **2007**, *22*, 5.
[86] Y. C. Hu, *J. Am. Ceram. Soc.* **2006**, *89*, 2949.
[87] J. W. Lee, J. H. Lee, E. J. Woo, H. Ahn, J. S. Kim, C. H. Lee, *Ind. Eng. Chem. Res.* **2008**, *47*, 5994.
[88] J. R. Niu, J. G. Deng, W. Liu, L. Zhang, G. Z. Wang, H. X. Dai, H. He, X. H. Zi, *Catal. Today* **2007**, *126*, 420.
[89] F. Gözüak, Y. Koseoglu, A. Baykal, H. Kavasa, *J. Magn. Magn. Mater.* **2009**, *321*, 2170.
[90] L. Q. Zhou, Y. G. Liang, L. Hu, X. Y. Han, Z. H. Yi, J. T. Sun, S. J. Yang, *J. Alloys Compd.* **2008**, *457*, 389.
[91] T. Y. Chen, K. Z. Fung, *J. Eur. Ceram. Soc.* **2008**, *28*, 803.
[92] N. Moskala, J. Morgiel, W. Pyda, *Mater. Sci.* **2008**, *26*, 331.
[93] M. Prades, H. Beltran, N. Maso, E. Cordoncillo, A. R. West, *J. Appl. Phys.* **2008**, *104*, 104118.
[94] Y. G. Su, L. P. Li, G. S. Li, *Chem. Mater.* **2008**, *20*, 6060.
[95] X. Wei, G. Xu, Z. H. Ren, Y. G. Wang, G. Shen, G. R. Han, *J. Cryst. Growth* **2008**, *310*, 4132.
[96] L. W. Zhang, H. B. Fu, C. Zhang, Y. F. Zhu, *J. Phys. Chem. C* **2008**, *112*, 3126.
[97] Q. Zhang, M. F. Zhu, Q. H. Zhang, Y. G. Li, H. Z. Wang, *Mater. Chem. Phys.* **2009**, *116*, 658.
[98] V. Polshettiwar, M. N. Nadagouda, R. S. Varma, *Aust. J. Chem.* **2009**, *62*, 16.
[99] F. Gao, Q. Y. Lu, X. K. Meng, S. Komarneni, *J. Mater. Sci.* **2008**, *43*, 2377.
[100] S. Komarneni, H. Katsuki, *Pure Appl. Chem.* **2002**, *74*, 1537.

[101] W. C. Conner, G. A. Tompsett, *J. Phys. Chem. B* **2008**, *112*, 2110.
[102] K. J. Rao, B. Vaidhyanathan, M. Ganguli, P. A. Ramakrishnan, *Chem. Mater.* **1999**, *11*, 882.
[103] I. Bilecka, P. Elser, M. Niederberger, *ACS Nano* **2009**, *3*, 467.
[104] W. W. Wang, Y. J. Zhu, *Inorg. Chem. Commun.* **2004**, *7*, 1003.
[105] P. L. Zhu, J. W. Zhang, Z. S. Wu, Z. J. Zhang, *Cryst. Growth Des.* **2008**, *8*, 3148.
[106] J. Fidelus, R. R. Piticescu, R. M. Piticescu, W. Lojkowski, L. Giurgiu, *Z. Naturforsch. B* **2008**, *63*, 725.
[107] L. Zhang, Y. J. Zhu, *Appl. Phys. A* **2009**, *97*, 847.
[108] S. Cho, S. H. Jung, K. H. Lee, *J. Phys. Chem. C* **2008**, *112*, 12769.
[109] M. S. Mohajerani, M. Mazloumi, A. Lak, A. Kajbafvala, S. Zanganeh, S. K. Sadrnezhaad, *J. Cryst. Growth* **2008**, *310*, 3621.
[110] Z. Q. Chen, W. K. Li, W. J. Zeng, M. S. Li, J. H. Xiang, Z. H. Zho, J. L. Huang, *Mater. Lett.* **2008**, *62*, 4343.
[111] A. B. Corradi, F. Bondioli, B. Focher, A. M. Ferrari, C. Grippo, E. Mariani, C. Villa, *J. Am. Ceram. Soc.* **2005**, *88*, 2639.
[112] K. L. Ding, Z. J. Miao, Z. M. Liu, Z. F. Zhang, B. X. Han, G. M. An, S. D. Miao, Y. Xie, *J. Am. Chem. Soc.* **2007**, *129*, 6362.
[113] Y. F. Li, H. F. Li, T. H. Li, G. L. Li, R. Cao, *Microporous Mesoporous Mater.* **2009**, *117*, 444.
[114] A. V. Murugan, V. Samuel, V. Ravi, *Mater. Lett.* **2006**, *60*, 479.
[115] E. K. Nyutu, C. H. Chen, P. K. Dutta, S. L. Suib, *J. Phys. Chem. C* **2008**, *112*, 9659.
[116] S. Ribbens, V. Meynen, G. Van Tendeloo, X. Ke, M. Mertens, B. U. W. Maes, P. Cool, E. F. Vansant, *Microporous Mesoporous Mater.* **2008**, *114*, 401.
[117] X. Wu, Q. Z. Jiang, Z. F. Ma, M. Fu, W. F. Shangguan, *Solid State Commun.* **2005**, *136*, 513.
[118] P. L. Zhang, S. Yin, T. Sato, *Appl. Catal. B* **2009**, *89*, 118.
[119] D. Koziej, F. Fischer, N. Kranzlin, W. R. Caseri, M. Niederberger, *ACS Appl. Mater. Interfaces* **2009**, *1*, 1097.
[120] J. H. Clark, F. E. I. Deswarte, T. J. Farmer, *Biofuels Bioprod. Biorefin.* **2009**, *3*, 72.
[121] S. Baldassari, S. Komarneni, E. Mariani, C. Villa, *Mater. Res. Bull.* **2005**, *40*, 2014.
[122] W. S. Dong, M. Y. Li, C. L. Liu, F. Q. Lin, Z. T. Liu, *J. Colloid Interface Sci.* **2008**, *319*, 115.
[123] E. Hammarberg, A. Prodi-Schwab, C. Feldmann, *Thin Solid Films* **2008**, *516*, 7437.
[124] J. Jouhannaud, J. Rossignol, D. Stuerga, *J. Solid State Chem.* **2008**, *181*, 1439.
[125] T. Krishnakumar, R. Jayaprakash, M. Parthibavarman, A. R. Phani, V. N. Singh, B. R. Mehta, *Mater. Lett.* **2009**, *63*, 896.
[126] E. Michel, D. Chaumont, D. Stuerga, *J. Colloid Interface Sci.* **2003**, *257*, 258.
[127] A. Srivastava, K. Jain, Rashmi, A. K. Srivastava, S. T. Lakshmikumar, *Mater. Chem. Phys.* **2006**, *97*, 85.
[128] V. Subramanian, W. W. Burke, H. W. Zhu, B. Q. Wei, *J. Phys. Chem. C* **2008**, *112*, 4550.
[129] G. C. Xi, Y. T. He, Q. Zhang, H. Q. Xiao, X. Wang, C. Wang, *J. Phys. Chem. C* **2008**, *112*, 11645.
[130] J. J. Zhu, J. M. Zhu, X. H. Liao, J. L. Fang, M. G. Zhou, H. Y. Chen, *Mater. Lett.* **2002**, *53*, 12.
[131] F. Heinroth, S. Munzer, A. Feldhoff, S. Passinger, W. Cheng, C. Reinhardt, B. Chichkov, P. Behrens, *J. Mater. Sci.* **2009**, *44*, 6490.
[132] X. L. Hu, J. C. Yu, J. M. Gong, Q. Li, G. S. Li, *Adv. Mater.* **2007**, *19*, 2324.
[133] I. Bilecka, I. Djerdj, M. Niederberger, *Chem. Commun.* **2008**, 886.
[134] I. Ganesh, R. Johnson, Y. R. Mahajan, A. Khan, S. S. Madhavendra, B. M. Reddy, *J. Mater. Res.* **2004**, *19*, 1015.
[135] H. D. Xie, D. Z. Shen, X. Q. Wang, G. Q. Shen, *Mater. Chem. Phys.* **2007**, *103*, 334.
[136] J. A. Collado, M. A. G. Aranda, A. Cabeza, P. Olivera-Pastor, S. Bruque, *J. Solid State Chem.* **2002**, *167*, 80.
[137] F. Conrad, Y. Zhou, M. Yulikov, K. Hametner, S. Weyeneth, G. Jeschke, D. Günther, J.-D. Grunwaldt, G. R. Patzke, *Eur. J. Inorg. Chem.* **2010**, 2036.
[138] T. Moeller, G. L. King, *J. Am. Chem. Soc.* **1953**, *75*, 6060.
[139] a) K. Faungnawakij, N. Shimoda, T. Fukunaga, R. Kikuchi, K. Eguchi, *Appl. Catal. A* **2008**, *341*, 139; b) G. A. Petrakovskii, K. S. Aleksandrov, L. N. Bezmaternikh, S. S. Aplesnin, B. Roessli, F. Semadeni, A. Amato, C. Baines, J. Bartolome, M. Evangelisti, *Phys. Rev. B* **2001**, *63*, 184425.
[140] V. Varadarajan, D. P. Norton, *Appl. Phys. A* **2006**, *85*, 117.
[141] R. Srinivasan, B. Chavillon, C. Doussier-Brochard, L. Cario, M. Paris, E. Gautron, P. Deniard, F. Odobel, S. Jobic, *J. Mater. Chem.* **2008**, *18*, 5647.
[142] T. Nakamura, S. Yanagida, Y. Wada, *Res. Chem. Intermed.* **2006**, *32*, 331.
[143] J. B. Wagner, O. Timpe, F. A. Hamid, A. Trunschke, U. Wild, D. S. Su, R. K. Widi, S. B. Abd Hamid, R. Schlögl, *Top. Catal.* **2006**, *38*, 51.
[144] N. R. Shiju, V. V. Guliants, *ChemPhysChem* **2007**, *8*, 1615.
[145] X. L. Hu, Y. J. Zhu, S. W. Wang, *Mater. Chem. Phys.* **2004**, *88*, 421.
[146] A. S. Shaporev, V. K. Ivanov, A. E. Baranchikov, Y. D. Tret'yakov, *Inorg. Mater.* **2007**, *43*, 35.
[147] T. Krishnakumar, R. Jayaprakash, N. Pinna, V. N. Singh, B. R. Mehta, A. R. Phani, *Mater. Lett.* **2009**, *63*, 242.
[148] S. Cho, B. R. Lee, H. J. Kim, D. H. Park, K. H. Lee, *Mater. Lett.* **2009**, *63*, 2025.
[149] L. H. Thompson, L. K. Doraiswamy, *Ind. Eng. Chem. Res.* **1999**, *38*, 1215.
[150] K. S. Suslick, D. J. Flannigan, *Annu. Rev. Phys. Chem.* **2008**, *59*, 659.
[151] K. S. Suslick, G. J. Price, *Annu. Rev. Mater. Sci.* **1999**, *29*, 295.
[152] T. J. Mason, *Sonochemistry: The Uses of Ultrasound in Chemistry*, Royal Society of Chemistry, Cambridge, **1990**.
[153] T. J. Mason, J. P. Lorimer, *Applied Sonochemistry*, Wiley-VCH, Weinheim, **2002**.
[154] S. Bhattacharyya, A. Gedanken, *Microporous Mesoporous Mater.* **2008**, *110*, 553.
[155] O. V. Abramov, A. Gedanken, Y. Koltypin, N. Perkas, I. Perelshtein, E. Joyce, T. J. Mason, *Surf. Coat. Technol.* **2009**, *204*, 718.
[156] U. T. Gonzenbach, A. R. Studart, E. Tervoort, L. J. Gauckler, *Angew. Chem.* **2006**, *118*, 3606; *Angew. Chem. Int. Ed.* **2006**, *45*, 3526.
[157] B. S. Murray, R. Ettelaie, *Curr. Opin. Colloid Interface Sci.* **2004**, *9*, 314.
[158] D. Grigoriev, R. Miller, D. Shchukin, H. Mohwald, *Small* **2007**, *3*, 665.
[159] A. L. Morel, S. I. Nikitenko, K. Gionnet, A. Wattiaux, J. Lai-Kee-Him, C. Labrugere, B. Chevalier, G. Deleris, C. Petibois, A. Brisson, M. Simonoff, *ACS Nano* **2008**, *2*, 847.
[160] J. H. Bang, K. S. Suslick, *J. Am. Chem. Soc.* **2007**, *129*, 2242.
[161] L. Zhu, Q. Li, J. Y. Li, X. D. Liu, J. Meng, X. Q. Cao, *J. Nanopart. Res.* **2007**, *9*, 261.
[162] N. Steunou, L. Bouhedja, S. Castro-Garcia, J. Livage, *High Pressure Res.* **2001**, *20*, 55.
[163] I. Djerdj, D. Sheptyakov, F. Gozzo, D. Arcon, R. Nesper, M. Niederberger, *J. Am. Chem. Soc.* **2008**, *130*, 11364.
[164] M. Sivakumar, T. Takami, H. Ikuta, A. Towata, K. Yasui, T. Tuziuti, T. Kozuka, D. Bhattacharya, Y. Iida, *J. Phys. Chem. B* **2006**, *110*, 15234.
[165] L. S. Zhang, W. Z. Wang, J. O. Yang, Z. G. Chen, W. Q. Zhang, L. Zhou, S. W. Liu, *Appl. Catal. A* **2006**, *308*, 105.
[166] D. S. Zhang, H. X. Fu, L. Y. Shi, C. S. Pan, Q. Li, Y. L. Chu, W. J. Yu, *Inorg. Chem.* **2007**, *46*, 2446.
[167] D. N. Srivastava, V. G. Pol, O. Palchik, L. Zhang, J. C. Yu, A. Gedanken, *Ultrason. Sonochem.* **2005**, *12*, 205.

[168] J. Pinkas, V. Reichlova, R. Zboril, Z. Moravec, P. Bezdicka, J. Matejkova, *Ultrason. Sonochem.* **2008**, *15*, 257.
[169] R. Abu Mukh-Qasem, A. Gedanken, *J. Colloid Interface Sci.* **2005**, *284*, 489.
[170] F. Dang, N. Enomoto, J. Hojo, K. Enpuku, *Ultrason. Sonochem.* **2009**, *16*, 649.
[171] V. G. Kumar, K. B. Kim, *Ultrason. Sonochem.* **2006**, *13*, 549.
[172] V. G. Kumar, D. Aurbuch, A. Gedanken, *Ultrason. Sonochem.* **2003**, *10*, 17.
[173] C. V. Krishnan, J. L. Chen, C. Burger, B. Chu, *J. Phys. Chem. B* **2006**, *110*, 20182.
[174] S. Majumdar, S. Chakraborty, P. S. Devi, A. Sen, *Mater. Lett.* **2008**, *62*, 1249.
[175] W. L. Guo, Z. M. Lin, X. K. Wang, G. Z. Song, *Microelectron. Eng.* **2003**, *66*, 95.
[176] K. Yang, J. M. Zhu, J. J. Zhu, S. S. Huang, X. H. Zhu, G. B. Ma, *Mater. Lett.* **2003**, *57*, 4639.
[177] H. Arami, M. Mazloumi, R. Khalifehzadeh, S. K. Sadmezhaad, *Mater. Lett.* **2007**, *61*, 4559.
[178] D. Qian, J. Z. Jiang, P. L. Hansen, *Chem. Commun.* **2003**, 1078.
[179] S. H. Jung, E. Oh, K. H. Lee, W. Park, S. H. Jeong, *Adv. Mater.* **2007**, *19*, 749.
[180] H. M. Xiong, D. G. Shchukin, H. Mohwald, Y. Xu, Y. Y. Xia, *Angew. Chem.* **2009**, *121*, 2765; *Angew. Chem. Int. Ed.* **2009**, *48*, 2727.
[181] L. Zhou, W. Z. Wang, L. S. Zhang, *J. Mol. Catal. A* **2007**, *268*, 195.
[182] M. Shang, W. Z. Wang, L. Zhou, S. M. Sun, W. Z. Yin, *J. Hazard. Mater.* **2009**, *172*, 338.
[183] D. P. Dutta, J. Manjanna, A. K. Tyagi, *J. Appl. Phys.* **2009**, *106*, 043915.
[184] W. Z. Lv, B. Liu, Q. Qiu, F. Wang, Z. K. Luo, P. X. Zhang, S. H. Wei, *J. Alloys Compd.* **2009**, *479*, 480.
[185] K. H. Kim, K. B. Kim, *Ultrason. Sonochem.* **2008**, *15*, 1019.
[186] J. Geng, J. J. Zhu, D. J. Lu, H. Y. Chen, *Inorg. Chem.* **2006**, *45*, 8403.
[187] A. Troia, M. Pavese, F. Geobaldo, *Ultrason. Sonochem.* **2009**, *16*, 136.
[188] T. Thongtem, A. Phuruangrat, S. Thongtem, *Appl. Surf. Sci.* **2008**, *254*, 7581.
[189] T. Thongtem, A. Phuruangrat, S. Thongtem, *J. Ceram. Process. Res.* **2008**, *9*, 189.
[190] R. Kalai Selvan, A. Gedanken, P. Anilkumar, G. Manikandan, C. Karunakaran, *J. Cluster Sci.* **2009**, *20*, 291.
[191] D. P. Dutta, R. Ghildiyal, A. K. Tyagi, *J. Phys. Chem. C* **2009**, *113*, 16954.
[192] M. Sivakumar, A. Towata, K. Yasui, T. Tuziuti, Y. Iida, *Curr. Appl. Phys.* **2006**, *6*, 591.
[193] C. L. Yu, J. C. Yu, *Mater. Sci. Eng. B* **2009**, *164*, 16.
[194] R. K. Selvan, A. Gedanken, *Nanotechnology* **2009**, *20*, 105602.
[195] *Ionic Liquids in Synthesis* (Eds.: P. Wasserscheid, T. Welton), 2nd ed., Wiley-VCH, Weinheim, **2008**.
[196] C. Chiappe, D. Pieraccini, *J. Phys. Org. Chem.* **2005**, *18*, 275.
[197] T. Welton, *Coord. Chem. Rev.* **2004**, *248*, 2459.
[198] R. Sheldon, *Chem. Commun.* **2001**, 2399.
[199] M. Antonietti, B. Smarsly, Y. Zhou in *Ionic Liquids in Synthesis*, *Vol. 2* (Eds.: P. Wasserscheid, T. Welton), 2nd ed., Wiley-VCH, Weinheim, **2002**, p. 609.
[200] X. Zhou, Z. X. Xie, Z. Y. Jiang, Q. Kuang, S. H. Zhang, T. Xu, R. B. Huang, L. S. Zheng, *Chem. Commun.* **2005**, 5572.
[201] a) Z. H. Li, A. Shkilnyy, A. Taubert, *Cryst. Growth Des.* **2008**, *8*, 4526; b) Z. Li, A. Gessner, J.-P. Richters, J. Kalden, T. Voss, C. Kübel, A. Taubert, *Adv. Mater.* **2008**, *20*, 1279.
[202] D. P. Liu, G. D. Li, Y. Su, J. S. Chen, *Angew. Chem.* **2006**, *118*, 7530; *Angew. Chem. Int. Ed.* **2006**, *45*, 7370.
[203] H. G. Zhu, J. F. Huang, Z. W. Pan, S. Dai, *Chem. Mater.* **2006**, *18*, 4473.
[204] I. Yavari, A. R. Mahjoub, E. Kowsari, M. Movahedi, *J. Nanopart. Res.* **2009**, *11*, 861.
[205] H. Kaper, F. Endres, I. Djerdj, M. Antonietti, B. M. Smarsly, J. Maier, Y. S. Hu, *Small* **2007**, *3*, 1753.
[206] W. J. Zheng, X. D. Liu, Z. Y. Yan, L. J. Zhu, *ACS Nano* **2009**, *3*, 115.
[207] L.-L. Li, W.-M. Zhang, Q. Yuan, Z.-X. Li, C.-J. Fang, L.-D. Sun, L.-J. Wan, C.-H. Yan, *Cryst. Growth Des.* **2008**, *8*, 4165.
[208] H. Kaper, M. G. Willinger, I. Djerdj, S. Gross, M. Antonietti, B. M. Smarsly, *J. Mater. Chem.* **2008**, *18*, 5761.
[209] Z. H. Li, P. Rabu, P. Strauch, A. Mantion, A. Taubert, *Chem. Eur. J.* **2008**, *14*, 8409.
[210] N. Recham, L. Dupont, M. Courty, K. Djellab, D. Larcher, M. Armand, J. M. Tarascon, *Chem. Mater.* **2009**, *21*, 1096.
[211] A. Zharkouskay, H. Lunsdorf, C. Feldmann, *J. Mater. Sci.* **2009**, *44*, 3936.
[212] H. Choi, Y. J. Kim, R. S. Varma, D. D. Dionysiou, *Chem. Mater.* **2006**, *18*, 5377.
[213] K. S. Yoo, H. Choi, D. D. Dionysiou, *Catal. Commun.* **2005**, *6*, 259.
[214] T. Nakashima, N. Kimizuka, *J. Am. Chem. Soc.* **2003**, *125*, 6386.
[215] Ref. [207].
[216] D. Chandra, N. Mukherjee, A. Mondal, A. Bhaumik, *J. Phys. Chem. C* **2008**, *112*, 8668.
[217] M. Al Zoubi, H. K. Farag, F. Endres, *J. Mater. Sci.* **2009**, *44*, 1363.
[218] Z. X. Li, L. L. Li, Q. Yuan, W. Feng, J. Xu, L. D. Sun, W. G. Song, C. H. Yan, *J. Phys. Chem. C* **2008**, *112*, 18405.
[219] T. Alammar, A. Birkner, A. V. Mudring, *Eur. J. Inorg. Chem.* **2009**, 2765.
[220] Y. H. He, D. Z. Li, Z. X. Chen, Y. B. Chen, X. Z. Fu, *J. Am. Ceram. Soc.* **2007**, *90*, 3698.
[221] G. Bühler, C. Feldmann, *Angew. Chem.* **2006**, *118*, 4982; *Angew. Chem. Int. Ed.* **2006**, *45*, 4864.
[222] T. Alammar, A. V. Mudring, *Mater. Lett.* **2009**, *63*, 732.
[223] X. D. Xu, M. Zhang, J. Feng, M. L. Zhang, *Mater. Lett.* **2008**, *62*, 2787.
[224] J. X. Xia, H. M. Li, Z. J. Luo, H. Shi, K. Wang, H. M. Shu, Y. S. Yan, *J. Phys. Chem. Solids* **2009**, *70*, 1461.
[225] S. W. Cao, Y. J. Zhu, *Acta Mater.* **2009**, *57*, 2154.
[226] W. W. Wang, Y. J. Zhu, *Cryst. Growth Des.* **2005**, *5*, 505.
[227] S. M. Liu, X. L. Qian, J. Z. Xiao, *J. Sol-Gel Sci. Technol.* **2007**, *44*, 187.
[228] D. Mangin, F. Puel, S. Veesler, *Org. Process Res. Dev.* **2009**, *13*, 1241.
[229] D. Erdemir, A. Y. Lee, A. S. Myerson, *Acc. Chem. Res.* **2009**, *42*, 621.
[230] M. A. Lovette, A. R. Browning, D. W. Griffin, J. P. Sizemore, R. C. Snyder, M. F. Doherty, *Ind. Eng. Chem. Res.* **2008**, *47*, 9812.
[231] J. A. Hinks, *Nucl. Instrum. Methods Phys. Res. Sect. B* **2009**, *267*, 3652.
[232] R. Sharma, *Microsc. Res. Tech.* **2009**, *72*, 144.
[233] J. D. Epping, B. F. Chmelka, *Curr. Opin. Colloid Interface Sci.* **2006**, *11*, 81.
[234] R. I. Walton, D. O'Hare, *Chem. Commun.* **2000**, 2283.
[235] A. K. Cheetham, C. F. Mellot, *Chem. Mater.* **1997**, *9*, 2269.
[236] H. Jensen, M. Bremholm, R. P. Nielsen, K. D. Joensen, J. S. Pedersen, H. Birkedal, Y. S. Chen, J. Almer, E. G. Sogaard, S. B. Iversen, B. B. Iversen, *Angew. Chem.* **2007**, *119*, 1131; *Angew. Chem. Int. Ed.* **2007**, *46*, 1113.
[237] G. Garnweitner, C. Grote, *Phys. Chem. Chem. Phys.* **2009**, *11*, 3767.
[238] D. R. Hummer, J. D. Kubicki, P. R. C. Kent, J. E. Post, P. J. Heaney, *J. Phys. Chem. C* **2009**, *113*, 4240.

[239] a) R. H. Sui, V. Thangadurai, C. P. Berlinguette, *Chem. Mater.* **2008**, *20*, 7022; b) R. H. Sui, A. S. Rizkallah, P. A. Charpentier, *Cryst. Growth Des.* **2008**, *8*, 3024.
[240] K. Biswas, N. Varghese, C. N. R. Rao, *J. Mater. Sci. Technol.* **2008**, *24*, 615.
[241] K. Biswas, B. Das, C. N. R. Rao, *J. Phys. Chem. C* **2008**, *112*, 2404.
[242] S. Fall, O. Konovalov, M. Maaza, A. C. Beye, A. Gibaud, *J. Appl. Crystallogr.* **2009**, *42*, 815.
[243] C. Lizandara-Pueyo, M. W. E. van den Berg, A. De Toni, T. Goes, S. Polarz, *J. Am. Chem. Soc.* **2008**, *130*, 16601.
[244] R. Viswanatha, H. Amenitsch, D. D. Sarma, *J. Am. Chem. Soc.* **2007**, *129*, 4470.
[245] Z. Hu, D. J. Escamilla Ramirez, B. E. Heredia Cervera, G. Oskam, P. C. Searson, *J. Phys. Chem. B* **2005**, *109*, 11209.
[246] T. Gao, H. Fjellvag, P. Norby, *Nanotechnology* **2009**, *20*, 055610.
[247] X. F. Shen, Y. S. Ding, J. C. Hanson, M. Aindow, S. L. Suib, *J. Am. Chem. Soc.* **2006**, *128*, 4570.
[248] M. Bremholm, M. Felicissimo, B. B. Iversen, *Angew. Chem.* **2009**, *121*, 4882; *Angew. Chem. Int. Ed.* **2009**, *48*, 4788.
[249] M. Bremholm, J. Becker-Christensen, B. Iversen, *Adv. Mater.* **2009**, *21*, 3572.
[250] A. Michailovski, J. D. Grunwaldt, A. Baiker, R. Kiebach, W. Bensch, G. R. Patzke, *Angew. Chem.* **2005**, *117*, 5787; *Angew. Chem. Int. Ed.* **2005**, *44*, 5643.
[251] Y. Zhou, N. Pienack, W. Bensch, G. R. Patzke, *Small* **2009**, *5*, 1978.
[252] A. M. Beale, G. Sankar, *Chem. Mater.* **2003**, *15*, 146.
[253] C. Kongmark, V. Martis, A. Rubbens, C. Pirovano, A. Lofberg, G. Sankar, E. Bordes-Richard, R. N. Vannier, W. Van Beek, *Chem. Commun.* **2009**, 4850.
[254] A. M. Beale, G. Sankar, *Chem. Mater.* **2006**, *18*, 263.
[255] a) D. R. Modeshia, R. J. Darton, S. E. Ashbrook, R. I. Walton, *Chem. Commun.* **2009**, 68; b) R. D. Fisher, R. I. Walton, *Dalton Trans.* **2009**, 8079.
[256] R. Kiebach, N. Pienack, M. E. Ordolff, F. Studt, W. Bensch, *Chem. Mater.* **2006**, *18*, 1196.
[257] Y. Du, K. M. Ok, D. O'Hare, *J. Mater. Chem.* **2008**, *18*, 4450.
[258] A. M. Beale, L. M. Reilly, G. Sankar, *Appl. Catal. A* **2007**, *325*, 290.
[259] B. L. Kirsch, E. K. Richman, A. E. Riley, S. H. Tolbert, *J. Phys. Chem. B* **2004**, *108*, 12698.
[260] F. Millange, C. Serre, N. Guillou, G. Ferey, R. I. Walton, *Angew. Chem.* **2008**, *120*, 4168; *Angew. Chem. Int. Ed.* **2008**, *47*, 4100.
[261] R. Enjalbert, G. Hasselmann, J. Galy, *J. Solid State Chem.* **1997**, *131*, 236.
[262] S. Russu, M. Tromp, N. Tsapatsaris, A. M. Beesley, S. L. M. Schroeder, M. T. Weller, J. Evans in *X-Ray Absorption Fine Structure-XAFS13*, *Vol. 882* (Eds.: B. Hedman, P. Painetta), American Institute of Physics, Melville, **2007**, p. 535.
[263] J. Wu, F. Duan, Y. Zheng, Y. Xie, *J. Phys. Chem. C* **2007**, *111*, 12866.
[264] L. H. Zhang, W. Z. Wang, Z. G. Chen, L. Zhou, H. L. Xu, W. Zhu, *J. Mater. Chem.* **2007**, *17*, 2526.
[265] Y. Y. Li, J. P. Liu, X. T. Huang, G. Y. Li, *Cryst. Growth Des.* **2007**, *7*, 1350.
[266] S. W. Liu, J. G. Yu, *J. Solid State Chem.* **2008**, *181*, 1048.
[267] F. Amano, K. Nogami, R. Abe, B. Ohtani, *J. Phys. Chem. C* **2008**, *112*, 9320.
[268] F. Amano, K. Nogami, R. Abe, B. Ohtani, *Chem. Lett.* **2007**, *36*, 1314.
[269] M. Avrami, *J. Chem. Phys.* **1941**, *9*, 177.
[270] L. Schlicker, R. Riedel, A. Gurlo, *Nanotechnology* **2009**, *20*, 495702.
[271] a) J. J. Rehr, R. C. Albers, *Rev. Mod. Phys.* **2000**, *72*, 621; b) M. A. Newton, A. J. Dent, J. Evans, *Chem. Soc. Rev.* **2002**, *31*, 83.
[272] H. Huwe, M. Fröba, *J. Synchrotron Radiat.* **2006**, *13*, 275.
[273] Y. Zhou, J.-D. Grunwaldt, F. Krumeich, K. Zheng, G. Chen, J. Stötzel, R. Frahm, G. R. Patzke, *Small* **2010**, *6*, 1173.
[274] J. D. Grunwaldt, M. Beier, B. Kimmerle, A. Baiker, M. Nachtegaal, B. Griesebock, D. Lützenkirchen-Hecht, J. Stotzeld, R. Frahm, *Phys. Chem. Chem. Phys.* **2009**, *11*, 8779.
[275] C. N. R. Rao, K. Biswas, *Annu. Rev. Anal. Chem.* **2009**, *2*, 435.
[276] S. Nikitenko, A. M. Beale, A. M. J. van der Eerden, S. D. M. Jacques, O. Leynaud, M. G. O'Brien, D. Detollenaere, R. Kaptein, B. M. Weckhuysen, W. Bras, *J. Synchrotron Radiat.* **2008**, *15*, 632.
[277] A. M. Beale, A. M. J. van der Eerden, S. D. M. Jacques, O. Leynaud, M. G. O'Brien, F. Meneau, S. Nikitenko, W. Bras, B. M. Weckhuysen, *J. Am. Chem. Soc.* **2006**, *128*, 12386.
[278] K. Byrappa, S. Ohara, T. Adschiri, *Adv. Drug Delivery Rev.* **2008**, *60*, 299.
[279] N. Iyi, K. Fujii, K. Okamoto, T. Sasaki, *Appl. Clay Sci.* **2007**, *35*, 218.
[280] Y. Du, D. O'Hare, *Inorg. Chem.* **2008**, *47*, 11839.
[281] R. G. Xie, Z. Li, X. G. Peng, *J. Am. Chem. Soc.* **2009**, *131*, 15457.
[282] R. Viswanatha, P. K. Santra, C. Dasgupta, D. D. Sarma, *Phys. Rev. Lett.* **2007**, *98*, 255501.
[283] F. Fan, Z. Feng, C. Li, *Acc. Chem. Res.* **2010**, *43*, 378.
[284] F. Fan, Z. Feng, K. Sun, M. Guo, Q. Guo, Y. Song, W. Li, C. Li, *Angew. Chem.* **2009**, *121*, 8899; *Angew. Chem. Int. Ed.* **2009**, *48*, 8743.
[285] F. Fan, Z. Feng, G. Li, K. Sun, P. Ying, C. Li, *Chem. Eur. J.* **2008**, *14*, 5125.
[286] S. Hamad, S. Cristol, C. R. A. Catlow, *J. Am. Chem. Soc.* **2005**, *127*, 2580.
[287] D. Zahn, *Phys. Rev. Lett.* **2004**, *92*, 4040801.
[288] J. Alejandre, J. P. Hansen, *Phys. Rev. E* **2007**, *76*, 061505.
[289] E. Arzt, *Acta Mater.* **1998**, *46*, 5611.
[290] G. Dehm, T. J. Balk, H. Edongue, E. Arzt, *Micoelectron. Eng.* **2003**, *70*, 412.
[291] P. A. Gruber, E. Arzt, R. Spolenak, *J. Mater. Res.* **2009**, *24*, 1906.
[292] P. Buffat, J. P. Borel, *Phys. Rev. A* **1976**, *13*, 2287.
[293] J. A. Forrest, K. Dalnoki-Veress, J. R. Stevens, J. R. Dutcher, *Phys. Rev. Lett.* **1996**, *77*, 2002.
[294] R. D. Priestley, C. J. Ellison, L. J. Broadbelt, J. M. Torkelson, *Science* **2005**, *309*, 456.
[295] G. F. Goya, T. S. Berquo, F. C. Fonseca, M. P. Morales, *J. Appl. Phys.* **2003**, *94*, 3520.
[296] W. Steinhögl, G. Schindler, G. Steinlesberger, M. Engelhardt, *Phys. Rev. B* **2002**, *66*, 075414.
[297] T. M. Shaw, S. Trolier-McKinstry, P. C. McIntyre, *Annu. Rev. Mater. Sci.* **2000**, *30*, 263.
[298] Q. A. Pankhurst, J. Connolly, S. K. Jones, J. Dobson, *J. Phys. D* **2003**, *36*, R167.
[299] R. Cornell, U. Schwertmann, *The Iron Oxides*, 2nd ed., Wiley-VCH, Weinheim, **2003**.
[300] Y. Ju-Nam, J. R. Lead, *Sci. Total Environ.* **2008**, *400*, 396.
[301] R. J. Aitken, M. Q. Chaudhry, A. B. A. Boxall, M. Hull, *Occup. Med.* **2006**, *56*, 300.
[302] K. Schmid, M. Riediker, *Environ. Sci. Technol.* **2008**, *42*, 2253.
[303] M. C. Floody, B. K. G. Theng, P. Reyes, M. L. Mora, *Clay Miner.* **2009**, *44*, 161.
[304] C. T. Yavuz, A. Prakash, J. T. Mayo, V. L. Colvin, *Chem. Eng. Sci.* **2009**, *64*, 2510.
[305] D. Horák, M. Babic, H. Mackova, M. J. Benes, *J. Sep. Sci.* **2007**, *30*, 1751.
[306] E. Palecek, M. Fojta, *Talanta* **2007**, *74*, 276.
[307] A. H. Lu, E. L. Salabas, F. Schüth, *Angew. Chem.* **2007**, *119*, 1242; *Angew. Chem. Int. Ed.* **2007**, *46*, 1222.
[308] M. M. Mojtahedi, M. S. Abaee, M. Eghtedari, *Appl. Organomet. Chem.* **2008**, *22*, 529.

[309] M. V. Barmatova, I. D. Ivanchikova, O. A. Kholdeeva, A. N. Shmakov, V. I. Zaikovskii, M. S. Mel'gunov, *J. Mater. Chem.* **2009**, *19*, 7332.
[310] Y. Lu, Y. D. Yin, B. T. Mayers, Y. N. Xia, *Nano Lett.* **2002**, *2*, 183.
[311] W. Stöber, A. Fink, E. Bohn, *J. Colloid Interface Sci.* **1968**, *26*, 62.
[312] A. P. Philipse, M. P. B. van Bruggen, C. Pathmamanoharan, *Langmuir* **1994**, *10*, 92.
[313] D. Yang, J. H. Hu, S. K. Fu, *J. Phys. Chem. C* **2009**, *113*, 7646.
[314] T. Hirakawa, S. Tanaka, N. Usuki, H. Kanzaki, M. Kishimoto, M. Kitamura, *Eur. J. Org. Chem.* **2009**, 789.
[315] J. Winkler, *Titandioxid*, Vincentz Network, Hannover, **2003**.
[316] D. Beydoun, R. Amal, G. K. C. Low, S. McEvoy, *J. Phys. Chem. B* **2000**, *104*, 4387.
[317] S. Watson, J. Scott, D. Beydoun, R. Amal, *J. Nanopart. Res.* **2005**, *7*, 691.
[318] S. Xu, W. Shangguan, J. Yuan, M. Chen, J. Shi, Z. Jiang, *Nanotechnology* **2008**, *19*, 095606.
[319] C. L. Fang, K. Qian, J. H. Zhu, S. B. Wang, X. X. Lv, S. H. Yu, *Nanotechnology* **2008**, *19*, 125601.
[320] H. A. Macleod, *Thin-Film Optical Filters*, 3rd ed., Institute of Physics, London, **2001**.
[321] J. D. Joannopoulos, S. G. Johnson, J. N. Winn, R. D. Meade, *Photonic Crystals—Molding the Flow of Light*, 2nd ed., Princeton University Press, Princeton, **2008**.
[322] M. E. Calvo, O. Sanchez-Sobrado, S. Colodrero, H. Miguez, *Langmuir* **2009**, *25*, 2443.
[323] S. Y. Choi, M. Mamak, G. von Freymann, N. Chopra, G. A. Ozin, *Nano Lett.* **2006**, *6*, 2456.
[324] S. Colodrero, M. Ocana, H. Miguez, *Langmuir* **2008**, *24*, 4430.
[325] J. Kobler, B. V. Lotsch, G. A. Ozin, T. Bein, *ACS Nano* **2009**, *3*, 1669.
[326] L. D. Bonifacio, B. V. Lotsch, D. P. Puzzo, F. Scotognella, G. A. Ozin, *Adv. Mater.* **2009**, *21*, 1641.
[327] D. P. Puzzo, L. D. Bonifacio, J. Oreopoulos, C. M. Yip, I. Manners, G. A. Ozin, *J. Mater. Chem.* **2009**, *19*, 3500.
[328] S. Colodrero, A. Mihi, L. Haggman, M. Ocana, G. Boschloo, A. Hagfeldt, H. Miguez, *Adv. Mater.* **2009**, *21*, 764.
[329] M. E. Calvo, S. Colodrero, T. C. Rojas, J. A. Anta, M. Ocana, H. Miguez, *Adv. Funct. Mater.* **2008**, *18*, 2708.
[330] M. Karaman, S. E. Kooi, K. K. Gleason, *Chem. Mater.* **2008**, *20*, 2262.
[331] X. L. Xu, S. A. Majetich, S. A. Asher, *J. Am. Chem. Soc.* **2002**, *124*, 13864.
[332] T. Druffel, K. B. Geng, E. Grulke, *Nanotechnology* **2006**, *17*, 3584.
[333] T. Druffel, N. Mandzy, M. Sunkara, E. Grulke, *Small* **2008**, *4*, 459.
[334] R. G. DeCorby, N. Ponnampalam, H. T. Nguyen, T. J. Clement, *Adv. Mater.* **2007**, *19*, 193.
[335] M. E. Calvo, O. S. Sobrado, G. Lozano, H. Miguez, *J. Mater. Chem.* **2009**, *19*, 3144.
[336] M. C. Fuertes, F. J. Lopez-Alcaraz, M. C. Marchi, H. E. Troiani, V. Luca, H. Miguez, G. Soler-Illia, *Adv. Funct. Mater.* **2007**, *17*, 1247.
[337] S. A. Wolf, A. Y. Chtchelkanova, D. M. Treger, *IBM J. Res. Dev.* **2006**, *50*, 101.
[338] *Magnetoelectronics* (Ed.: M. Johnson), Elsevier, Amsterdam, **2004**.
[339] *Semiconductors and Semimetals* (Ed.: E. R. Weber), Elsevier, Amsterdam, **2008**.
[340] J. Cibert, J. F. Bobo, U. Luders, *C. R. Phys.* **2005**, *6*, 977.
[341] T. Dietl, *Semicond. Sci. Technol.* **2002**, *17*, 377.
[342] J. Keller, PhD Thesis, Rheinisch-Westfälische Technische Hochschule Aachen (Aachen), **2007**.
[343] H. Ohno, *Science* **1998**, *281*, 951.
[344] J. M. D. Coey, S. A. Chambers, *MRS Bull.* **2008**, *33*, 1053.
[345] S. A. Chambers, *Surf. Sci. Rep.* **2006**, *61*, 345.
[346] J. M. D. Coey, K. Wongsaprom, J. Alaria, M. Venkatesan, *J. Phys. D* **2008**, *41*, 134012.
[347] R. Seshadri, *Curr. Opin. Solid State Mater. Sci.* **2005**, *9*, 1.
[348] M. A. Garcia, E. F. Pinel, J. de La Venta, A. Quesada, V. Bouzas, J. F. Fernandez, J. J. Romero, M. S. M. Gonzalez, J. L. Costa-Kramer, *J. Appl. Phys.* **2009**, *105*, 013925.
[349] M. Snure, D. Kumar, A. Tiwari, *JOM* **2009**, *61*, 72.
[350] S. A. Chambers, *Adv. Mater.* **2010**, *22*, 219.
[351] H. J. Xu, H. C. Zhu, X. D. Shan, Y. X. Liu, J. Y. Gao, X. Z. Zhang, J. M. Zhang, P. W. Wang, Y. M. Hou, D. P. Yu, *J. Phys. Condens. Matter* **2010**, *22*, 10.
[352] M. A. Garcia, J. M. Merino, E. F. Pinel, A. Quesada, J. de La Venta, M. L. R. Gonzalez, G. R. Castro, P. Crespo, J. Llopis, J. M. Gonzalez-Calbet, A. Hernando, *Nano Lett.* **2007**, *7*, 1489.
[353] S. G. Ray, S. S. Daube, G. Leitus, Z. Vager, R. Naaman, *Phys. Rev. Lett.* **2006**, *96*, 036101.
[354] A. Hernando, P. Crespo, M. A. Garcia, E. F. Pinel, J. de La Venta, A. Fernandez, S. Penades, *Phys. Rev. B* **2006**, *74*, 052403.

